Molecular Pharmacology Fast Forward. Published on September 11, 2007 as doi:10.1124/mol.107.038265

The Roof and Floor of the Muscarinic Binding Pocket: Variations in the Binding Modes of Orthosteric Ligands

J. Alex Goodwin, Edward C. Hulme, Christopher J. Langmead and Ben G. Tehan

Division of Physical Biochemistry, MRC National Institute for Medical Research, Mill Hill, London NW7 1AA, U.K.(ECH) and GlaxoSmithKline, New Frontiers Science Park, Harlow, Essex CM19 5AW, U.K. (JAG ,CJL, BT)

Molecular Pharmacology Fast Forward. Published on September 11, 2007 as DOI: 10.1124/mol.107.038265
This article has not been copyedited and formatted. The final version may differ from this version.

Running title:

The Roof and Floor of the Muscarinic Binding Pocket.

Address correspondence to:

Dr. E.C. Hulme,

Division of Physical Biochemistry,

MRC National Institute for Medical Research,

Mill Hill,

London NW7 1AA, U.K.

Tel: 44-208-816-2057

Fax: 44-208-906-4477

Email: ehulme@nimr.mrc.ac.uk

Abbreviations:

mAChR, muscarinic acetylcholine receptor; TM, transmembrane domain; ECL extracellular loop; PhI , phosphoinositide; n_H, Hill coefficient ; ACh, acetylcholine; NMS, (-)-N-methyl scopolamine; [^{3}H]NMS, l-[N-methyl-^{3}H]Scopolamine methyl chloride; QNB, (-)-3-quinuclidinyl benzilate: [^{3}H]QNB, l-Quinuclidinyl[phenyl -4-^{3}H] benzilate; HEPES, 4-(2-hydroxyethyl)-1-piperazineethanesulfonic acid.

Text pages: 46; Figures: 8; References: 40; Abstract: 248 words; Introduction: 750 words; Discussion: 1495 words; Supplementary tables:5.

Molecular Pharmacology Fast Forward. Published on September 11, 2007 as DOI: 10.1124/mol.107.038265
This article has not been copyedited and formatted. The final version may differ from this version.

ABSTRACT.

Alanine substitution mutagenesis has been used to investigate residues that make up the roof and floor of the muscarinic binding pocket, and regulate ligand access. We mutated the amino acids in the second extra-cellular loop of the M_1 mAChR that are homologous to the cis-retinal contact residues in rhodopsin, the disulfide-bonded Cys178 and Cys98 that anchor the loop to trans-membrane helix 3, the adjoining acidic residue Asp99, and the conserved aromatic residues Phe197 and Trp378 in the trans-membrane domain. The effects on ligand binding, kinetics and receptor function suggest that the second extra-cellular loop does not provide primary contacts for orthosteric ligands, including acetylcholine, but that it does contribute to micro-domains that are important for the conformational changes that accompany receptor activation. Kinetic studies suggest that the disulfide-bond between Cys98 and Cys178 may contribute to structures that regulate the access of positively-charged ligands such as N-methyl scopolamine to the binding pocket. Asp99 may act as a gatekeeper residue to this channel. In contrast, the bulkier lipophilic ligand 3-quinuclidinyl benzilate may require breathing motions of the receptor to access the binding site. Trp378 is a key residue for receptor activation as well as binding, whilst Phe197 represents the floor of the N-methyl scopolamine binding pocket, but does not interact with acetylcholine or 3-quinuclidinyl benzilate. Differences between the binding modes of N-methyl scopolamine, 3-quinuclidinyl benzilate and acetylcholine have been modelled. While the head-groups of these ligands occupy overlapping volumes within the binding site, their side-chains may follow significantly different directions.

Molecular Pharmacology Fast Forward. Published on September 11, 2007 as DOI: 10.1124/mol.107.038265
This article has not been copyedited and formatted. The final version may differ from this version.

Most of the amino acids that contribute to the orthosteric binding site of the muscarinic acetylcholine receptors (mAChRs) are in the trans-membrane (TM) domain. Point mutations (Wess, 1996; Heitz *et al.*, 1999), particularly alanine-scanning (Hulme *et al.*, 2003), have been particularly useful in identifying them. The putative contacts made by the inverse agonist (-)-N-methyl scopolamine (NMS) with the TM domain of the M_1 mAChR are homologous to the contacts of ground-state rhodopsin with cis-retinal (Palczewski *et al.*, 2000; Li *et al.*, 2004), with the exception of Trp157 in TM4 (Lu *et al.*, 2001) (residue 4.57 using the notation of (Ballesteros and Weinstein, 1995)).

In rhodopsin, the second extra-cellular loop (ECL2) forms an anti-parallel β-hairpin in which the inner strand is disulfide bonded to the top of TM3. The disulfide bond is a conserved feature of most of the rhodopsin-related GPCRs including the M_1 mAChR, where Cys98 and Cys178 are the linked residues (Kurtenbach *et al.*, 1990). Thus ECL2 is anchored within the trans-membrane domain. In rhodopsin, in addition to the conserved Cys187 (designated position 0) amino acid side chains at positions -6,-1, +1, +2 and +4 contribute to the retinal environment, delimiting the top of the binding site (Li *et al.*, 2004). At position -6, Glu181 may be the ancestral counter-ion for the retinal Schiff's base (Terakita *et al.*, 2004), possibly still playing this role in the metarhodopsin-1 intermediate (Ludeke *et al.*, 2005). No precise homologue of this residue exists in the M_1 mAChR where Arg171 and Thr172 are inserted C-terminal to Glu170 (position -8). The other retinal contact residues lie close to the polyene chain. Their homologues in the M_1 mAChR are Gln177, Cys178, Tyr179, Ile180 and Phe182.

Molecular Pharmacology Fast Forward. Published on September 11, 2007 as DOI: 10.1124/mol.107.038265
This article has not been copyedited and formatted. The final version may differ from this version.

Five of these eight positions are conserved across the vertebrate mAChR subtypes. Ala-substitution of three (Arg171, Thr172 and Phe182 human M_1 mAChR) reduced NMS or ACh affinity by 3-fold or less; effects on receptor signaling were not determined (Matsui *et al.*, 1995). In the M_1 mAChR, mutation of the disulfide-bonded Cys178 and its partner Cys98 to Ser abolished binding and signaling (Savarese *et al.*, 1992) but the less disruptive Ala mutants have not been studied. In the M_3 mAChR Ala-substitutions of the homologous cysteines reduced the affinity of NMS by 50-800-fold, of carbachol by more than 100-fold and the potency of the carbachol-induced phosphoinositide (PhI) response by 20,000-fold (Zeng *et al.*, 1999), although a very recent study of the M_2 and M_3 mAChRs suggests smaller effects (Huang and Ellis, 2007).

At the bottom of the binding site of rhodopsin, Trp265 (6.48) and Tyr268 (6.51) make the single largest contribution to the burial of cis-retinal surface area (Li *et al.*, 2004; Palczewski *et al.*, 2000). The key Trp residue at 6.48 has been mutated to Ala and/or Phe in M_1, M_2 and M_3 mAChRs (Wess *et al.*, 1993; Bourdon *et al.*, 1997; Heitz *et al.*, 1999), but no fully coherent data set that includes both binding and functional data has been obtained for the Ala mutant. The functional role of Phe197 (5.47), homologous to Phe212 which forms the base of the binding pocket for the β-ionone ring of cis-retinal, has not been studied in the mAChRs although it was a target for non-conservative inactivating mutations in a recent random mutagenesis study on the M_3 mAChR (Li *et al.*, 2007).

Molecular Pharmacology Fast Forward. Published on September 11, 2007 as DOI: 10.1124/mol.107.038265
This article has not been copyedited and formatted. The final version may differ from this version.

Here we report the effects on binding and signaling of Ala-substitution of the residues in ECL2 of the M_1 mAChR that are homologous to the retinal contact sites in rhodopsin, including the disulfide-bonded Cys178. Additionally, we have obtained functional data for the mutants previously studied by binding alone (Matsui *et al.*, 1995), and have mutated Cys98 to disrupt the disulfide bond that anchors ECL2 to the top of TM3. The results, interpreted by molecular modelling, indicate that residues in ECL2 make minimal direct contacts with the antagonists NMS and (-)-3-quinuclidinyl benzilate (QNB), or with the agonist ACh in the bound state, but that the integrity of several conserved ECL2 residues, particularly Cys178, is important for ACh-induced signal transduction. Kinetic studies suggest that ECL2, assisted by Asp99 (3.26), a residue previously studied by Asn-substitution (Fraser *et al.*, 1989), may contribute to structures that regulate the access of ligands to the trans-membrane binding pocket. Phe197, at the bottom of the orthosteric binding site, is important for the binding of NMS but not QNB and ACh, suggesting that the side-chains of these ligands follow different paths within the binding site. Trp378 interacts with all three ligands, and has a major role in transmitting the ACh-induced signal.

Molecular Pharmacology Fast Forward. Published on September 11, 2007 as DOI: 10.1124/mol.107.038265
This article has not been copyedited and formatted. The final version may differ from this version.

Materials and Methods

Equilibrium binding assays and phosphoinositide functional assays were carried out as described previously, with small variations (Jones *et al.*, 1995; Lu *et al.*, 1997; Lu and Hulme, 1999;)

Materials. [^{3}H]NMS (l-[N-methyl-^{3}H]Scopolamine methyl chloride; 84 Ci/mmol), [^{3}H]QNB (l-Quinuclidinyl[phenyl -4-^{3}H] benzilate, 42-48 Ci/mmol) and myo-D-[^{3}H]inositol (80 Ci/mmol) were purchased from Amersham Corp. Unlabelled ligands ((-)-N-methylscopolamine bromide, acetylcholine bromide, atropine) were from Sigma-Aldrich. The QuickChange™ kit was from Stratagene.

Mutagenesis and expressionof receptors. Briefly, residues of the rat M_1 mAChR were mutated to Ala or Asn using the QuickChange™ method. Mutant receptors, cloned into the pCD expression vector, and validated by di-deoxy sequencing, were transiently expressed in COS-7 cells by electroporation (BioRad Gene Pulser, 15 µg DNA, 260 V, 960 µF). Membrane preparations were made after 72 h as described previously. Where necessary, expression levels of poorly-expressed mutant receptors were rescued by treatment of the cultured cells with atropine (10^{-6} M) for 48 h before washing and harvesting for membrane preparations, or phosphoinositide turnover assays, as described previously (Lu and Hulme, 1999). The mutants W164A, Q165A, G169A, T172A, Q181A and S184A (hM_1 background) were the kind gift of Dr. Nigel Birdsall.

Molecular Pharmacology Fast Forward. Published on September 11, 2007 as DOI: 10.1124/mol.107.038265
This article has not been copyedited and formatted. The final version may differ from this version.

Equilibrium Binding and functional assays. Binding of (-)-N-[^{3}H]methylscopolamine ([^{3}H]NMS) and (-)-[^{3}H]quinuclidinyl benzilate ([^{3}H]QNB) to membrane preparations (15-30 µg membrane protein/ml) was measured at 30 ^{o}C in a buffer containing 20 mM Na-Hepes, 100 mM NaCl and 1 mM $MgCl_2$, pH 7.5 using an assay volume of 1 ml and an incubation time of 2 h ([^{3}H]-NMS)-4 h ([^{3}H]QNB). Non-specific binding was defined with 1 µM atropine. Assays were performed in quadruplicate. The binding reaction was terminated by rapid filtration on a Brandel or TomTec cell harvester. The mean expression level of the wild-type receptor was 1.84 ± 0.52 pmol [^{3}H]NMS binding sites/mg protein (mean ± SD). The expression of [^{3}H]QNB binding sites was up to 40 % higher in direct comparisons. We have previously reported that the quaternary antagonist NMS inhibits ca. 20 % of [^{3}H]QNB binding sites with low affinity possibly reflecting the penetration of the more lipophilic tertiary antagonist into sealed vesicles containing receptors inaccessible to [^{3}H]NMS (Ward *et al.*, 1999). Low affinity sites were not seen in competition experiments with the tertiary analogue scopolamine (S.D.C. Ward, Ph.D. Thesis, University of London, 1999). In the present experiments, 90 ± 1 % (n=5) of the wild type [^{3}H]QNB binding sites showed high affinity (pK_d = 9.6 ±0.18) inhibition by (-)-NMS, the remainder having a pK_d of ca. 6. The W378A mutant also gave 87 ± 2.4 % of higher affinity sites. The higher affinity binding constant, was used in further analysis. We have not further investigated the balance of the apparent discrepancy in binding capacity in this study, and cannot exclude more complex explanations.

Molecular Pharmacology Fast Forward. Published on September 11, 2007 as DOI: 10.1124/mol.107.038265
This article has not been copyedited and formatted. The final version may differ from this version.

The binding of ACh was measured by inhibition of the binding of radioligand concentrations ranging from 10^{-11}-$3x10^{-9}$ M as appropriate for the mutant and radioligand combination. NMS binding to low-affinity mutants that retained significant affinity for [^{3}H]QNB was measured similarly. ACh-stimulated total PhI turnover was assayed for 30 min at 37º C in Krebs-bicarbonate solution supplemented with 10 mM LiCl following prelabeling of the transfected COS-7 cells grown in 12-well plates with [^{3}H]inositol (1μCi/ml) for 48 h. The accumulation of total [^{3}H]inositol phosphates was measured (Jones *et al.*, 1995) . Assays were performed in triplicate.

Radioligand dissociation assays. Membranes were labelled to equilibrium by incubation with [^{3}H]NMS (3 x 10^{-9} M) or [^{3}H]QNB (3 x 10^{-10} M) for 2 or 4 h respectively. Dissociation was initiated by a 10-fold dilution into 10^{-5} M unlabeled NMS, and binding assayed at specified time points.

Data analysis. Saturation binding curves or self-competition curves for [^{3}H]antagonists were fitted to a one-site model of binding using SigmaPlot 8.0 or 10.0 to yield a total concentration of binding sites and an affinity constant. The results are expressed as pK_d. Expression levels (R_T) were normalised to simultaneously-transfected wild-type controls. Inhibition curves for ACh and other ligands were fitted to the Hill equation to yield an experimental pIC_{50} value and a slope factor (n_H).The experimental pIC_{50} values were corrected for the Cheng-Prusoff shift, as necessary, to yield the tabulated corrected pIC_{50} values. Some ACh binding curves were also fitted to a two-site

Molecular Pharmacology Fast Forward. Published on September 11, 2007 as DOI: 10.1124/mol.107.038265
This article has not been copyedited and formatted. The final version may differ from this version.

model of binding providing high and low affinity binding constants, and the associated proportions of binding sites.

In addition, a dimeric receptor model of binding was used to analyse certain experiments (Hulme, 2006). This took the form

$$[^3H]NMS\ bound/R_T = T1/T2 \text{ where}\ldots\ldots\ldots\ldots..(1)$$

$$T1 = K_{L1}.L+K_{A1}.K_{L3}.A.L+K_{L1}.K_{L2}.L^2\ldots\ldots\ldots\ldots\ldots\ldots\ldots.(2)$$

$$T2 = 1+2.K_{L1}.L+K_{L1}.K_{L2}.L^2+2.K_{A1}.K_{L3}.A.L+2.K_{A1}.A+K_{A1}.K_{A2}.A^2\ldots\ldots\ldots.(3)$$

[^{3}H]NMS bound is the measured concentration of specifically-bound [^{3}H]NMS. R_T is the total concentration of [^{3}H]NMS binding sites. K_{L1} and K_{L2} represent the intrinsic affinity constants for the binding of the first and second molecule of [^{3}H]NMS to the protomers of the presumed receptor dimer. This was assumed to occur without cooperativity, so that K_{L1} and K_{L2} were fixed at the values determined in direct binding experiments. Fitting the above expression to the ACh inhibition curve allowed K_{A1} and K_{A2}, the intrinsic affinity constants for the binding of the first and second molecules of ACh to be estimated, as well as the affinity constant K_{L3} for binding of [^{3}H]NMS to the singly ACh-occupied dimer. These values were obtained in a logarithmic form.

Radioligand dissociation time courses were fitted to single (or, where appropriate double) exponential functions yielding a dissociation rate constant, k_{off}, the initial concentration of bound radioligand, and the level of radioligand binding after full dissociation, which was equivalent to the level of non-specific binding.

Molecular Pharmacology Fast Forward. Published on September 11, 2007 as DOI: 10.1124/mol.107.038265
This article has not been copyedited and formatted. The final version may differ from this version.

PhI dose-response curves were fitted to a four-parameter logistic function, yielding a pEC_{50} (- log M) value and basal and maximum responses (E_{basal}, E_{max}). Slope factors were close to 1.0. In these experiments, E_{Max} was 3020 ± 430 dpm/assay (n=22) for the wild- type rM_1 receptor, and 4200 ±1020 (n=5) for the wild-type hM_1 receptor. The ratios of E_{Max} to E_{Basal} were 6.4 ±0.8 and 3.9 ±1.3 respectively. These values are not significantly different (P>0.11). Similarly, the pEC_{50} values were very similar (6.96 ±0.06, rM_1; 7.07 ± 0.16, hM_1). For the combined data set, the mean ± SEM ACh-independent signaling activity of the wild-type receptor was 477 ± 96 dpm, and the mean ACh-stimulated maximum activity was 2993 ± 462 dpm/assay (n=27), after subtraction of the null-transfection background (E_{Null}, 250 ± 23 dpm).

For the combined wild-type data set, E_{Basal} was correlated with E_{Max} over a wide range of values (correlation coefficient = 0.67, n=27, P<0.001). This proportionality suggests that the large variations in the responses, indicated by the high SEMs, may reflect differences in the density, efficiency of transfection of the cells, and efficiency of [^{3}H]inositol labelling of the phosphoinositide pool dependent on the state of the cells. In contrast, the pEC_{50} values for ACh showed little variation and were not correlated with the E_{Max} values.

To compensate for these variations, values of E_{Basal} and E_{Max} were determined relative to wild-type values obtained from contemporaneous controls. To take a specific example, for the C98A mutant, E_{Max} values in three independent experiments were 2973,

Molecular Pharmacology Fast Forward. Published on September 11, 2007 as DOI: 10.1124/mol.107.038265
This article has not been copyedited and formatted. The final version may differ from this version.

1749 and 1859 dpm; the corresponding E_{Max} values for the wild type rM_1 in simultaneous parallel transfections were 8031, 3111 and 4678 dpm yielding ratios of 0.37, 0.56 and 0.40, the mean of which is 0.443 ± 0.06. After the application of a correction for the irreducible background PhI signal, measured in null-transfections, which was assumed to be the same for wild type and mutant transfections, this became 0.40 ± 0.07. The correction takes the form

$$(E_{Max},mutant/E_{Max,}wild\text{-}type)cor = (E_{Max},mutant/E_{Max,}wild\ type)(1+r) - r.....(4)$$

where r is the ratio $E_{Null}/(E_{Max},wild\text{-}\ type\text{-}E_{Null})$, having a value of 0.083 for the combined rM_1 and hM_1 data set. A similar correction was applied to the E_{Basal} ratios, for which r = 0.52. The resulting values are tabulated, as % of wild-type, in supplementary Table 3.

Values of the signaling efficacy of the ACh-receptor complex (e_A), adjusted for variations in receptor expression and background signaling, were calculated using equations (Lu and Hulme, 1999; Hulme, 2006) that are based on the free association of receptors and G-proteins in the cell membrane (Azpiazu and Gautam, 2004).

$$e_A = ((IC_{50}/EC_{50}(1\text{-}B)) -1)/R_T \ldots.(5)$$

when the E_{max} value of the mutant (as a fraction of the wild-type receptor) is greater than 0.9 or

$$e_A = (E_{Max}/(1\text{-}E_{Max}))/R_T\ldots\ldots\ldots\ldots\ldots\ldots(6)$$

Molecular Pharmacology Fast Forward. Published on September 11, 2007 as DOI: 10.1124/mol.107.038265
This article has not been copyedited and formatted. The final version may differ from this version.

when the E_{Max} of the mutant is less than 0.9. In equation 5, the parameter *B* represents receptor-dependent basal signaling calculated as a fraction of the wild-type ACh-stimulated maximum signal, and had a mean value of 0.16 for the wild-type mAChR in these experiments. The two equations yield equivalent results, but when the potency ratio IC_{50}/EC_{50} is large, E_{Max} is close to 1; conversely, when E_{Max} is substantially less than 0.9, $IC_{50} \approx EC_{50}$. e_A values computed for the mutants were expressed relative to the wild-type receptor.

If the signaling unit is actually a dimer in which both subunits must be occupied to produce a maximum signal, as is the case for the mGluR (Kniazeff *et al.*, 2004), these expressions yield values which represent the geometric mean of the values for the individual subunits.

Statistical Analysis. Experiments were repeated at least 3 times. Values are tabulated as mean ± SEM. Statistical comparisons of affinity and rate constants for mutants and wild-type controls were carried out by 1-way ANOVA followed by Dunnett's post-hoc test, backed up by paired Students t-tests in marginal cases. Where values, such as expression levels, had been normalised to the wild-type control, 2-tailed t-tests were used to ascertain the level of significance of differences from the wild-type.

Molecular modelling.

Molecular Pharmacology Fast Forward. Published on September 11, 2007 as DOI: 10.1124/mol.107.038265
This article has not been copyedited and formatted. The final version may differ from this version.

Construction of the M_1 model. The initial model of the TM domain of human M_1 receptor was constructed by homology with the published X-ray crystal structure of bovine rhodopsin (Palczewski *et al.*, 2000). Alignment between the M_1 receptor sequence and bovine rhodopsin was based on the "classical" motifs found in each TM region, the asparagine in TM1, the aspartate in TM2, the "DRY" motif (ERY in rhodopsin) of TM3, the tryptophan in TM4, and the conserved prolines in TM5, TM6 and TM7. These alignments were used, with the standard homology modelling tools in the Quanta program to construct the seven helical bundle domain of the M_1 receptor. The extracellular loop regions were subsequently added using a procedure developed "in house", which makes use of a combined distance geometry sampling and molecular dynamics simulation (Blaney *et al.*, 2001). The side-chains of this model were then refined using the Karplus standard rotamer library (Dunbrack and Karplus, 1993). The final model was optimised fully (500 steps of Steepest Descent (SD) followed by 5000 steps of Adopted Basis Newton Raphson (ABNR)) with the CHARMM force field using helical distance constraints between the *ith* and *i+4th* residues (except proline) within a range of 1.8Å-2.5Å, to maintain the backbone hydrogen bonds of the helix bundle. A more in-depth overview of how a similar Family A aminergic receptor, the $5HT_{2A}$ receptor, was built is covered in a recent publication (Blaney, 2006).

Ligand docking studies. Ligand molecules were built and optimized within Spartan (SPARTAN SGI, version 5.1.3; Wavefunction, Inc.: Irvine, CA.) using an AM1 Hamiltonian. The atom-centered charges for the ligands, used in the docking studies,

Molecular Pharmacology Fast Forward. Published on September 11, 2007 as DOI: 10.1124/mol.107.038265
This article has not been copyedited and formatted. The final version may differ from this version.

were natural atomic orbital charges calculated at the Hartree-Fock level within Spartan, using a 6-31G* basis set.

Ligands were docked into the receptor model manually using a variety of low energy starting conformations. Adjustments of the receptor protein side-chains were made where necessary, always ensuring that these sidechains were only in allowed rotameric states (Dunbrack and Karplus, 1993). Once again, full optimisation of the receptor-ligand complexes was performed using CHARMM, the only constraints used being those which maintained the hydrogen bonding pattern of the helical bundle and the charge-charge interaction between the basic nitrogen of our ligand species and the acidic head-group of the Asp3.32 on TM3. This procedure allows full relaxation of both the ligand and the whole protein, something which is not possible with automated docking procedures.

The interaction energies between the ligand and individual amino acid residues were calculated by energy de-convolution and represent the summed steric and electrostatic contributions from all of the atoms in the residues interacting with the ligand. The force field used was CHARMM. Prior to calculating the interaction energies the complex was minimized using a Steepest Descent (SD) algorithm followed by a Newton-Raphson (ABNR) algorithm, the nonbonded cutoff was 15 angstroms and the constant dielectric epsilon was set to 5 during both the minimization steps and energy calculation.

The pKb of the basic nitrogen atom of QNB was calculated using the Advanced Chemistry Development pKa calculator (www.acdlabs.com).

Molecular Pharmacology Fast Forward. Published on September 11, 2007 as DOI: 10.1124/mol.107.038265
This article has not been copyedited and formatted. The final version may differ from this version.

Results

^{3}H-Labeled antagonist binding and receptor expression levels. The effects of the mutations on the expression of mAChR binding sites were measured by saturation binding assays using both [^{3}H]NMS and [^{3}H]QNB. Full details are given in supplementary Table 1. Where measurements were made with both antagonists, the expression levels of binding sites relative to wild-type were not significantly different, with the possible exception of F182A (P=0.03). The weighted means of the two sets of measurements are plotted in Fig. 1a.

Ala-substitutions of individual amino acid residues in ECL2 reduced M_1 mAChR expression levels by a maximum of 50 % relative to wild-type. In contrast, it was difficult or impossible to measure specific binding of the radioligands to mutants of Cys178, Cys98 and Phe197. In the case of C178A, the best case, the maximum observed level of binding was 12 ± 3 % of wild type (n=3). This increased to 40-50 % after treatment of the transfected cells with atropine (10^{-6} M) for 48 h before washing and harvesting. The expression levels of C98A, C98A/C178A, and F197A were also raised to between 15 and 30 % of wild-type (Fig. 1a). The ability of atropine to act as a "pharmacological chaperone" for poorly-expressed mutants has been described previously (Lu and Hulme, 1999).

Ala-substitution of the ECL2 loop residues Arg171, Tyr179, Ile180 and Phe182 marginally reduced the affinity of NMS from the wild-type value of 6.6 ± 0.5 x 10^{9} M^{-1}

Molecular Pharmacology Fast Forward. Published on September 11, 2007 as DOI: 10.1124/mol.107.038265
This article has not been copyedited and formatted. The final version may differ from this version.

(Fig. 1b). The maximum effect was 5-fold (R171A). The effects of R171A and F182A agree with published data for the hM_1 mAChR (Matsui *et al.*, 1995) but differ from a recent study on the M_3 mAChR (Scarselli *et al.*, 2007). These mutations did not significantly affect the affinity of QNB ($2.63 \pm 0.9 \times 10^{10}$ M^{-1}). Single and double substitution of Cys98 and Cys178 reduced the affinities of both NMS (Fig. 2a) and QNB (Fig. 1b) by 10-20-fold, as did the non-conservative substitution C178N.

In contrast, the mutation of Asp99 (TM3), Phe197 (TM5) and Trp378 (TM6) decreased the affinity of NMS by 8, 37 and 370-fold respectively, but of these only W378A significantly reduced the affinity of QNB, by 9-fold (Fig. 1b).

Acetylcholine binding. Consistent with previous reports, the binding of ACh to wild-type M_1 mAChRs was described by a slightly-flattened binding isotherm with a mean apparent affinity constant of $5.8 \pm 1.3 \times 10^4$ M^{-1}, and a mean Hill coefficient of 0.85, slightly but significantly less than 1.0 ($P<0.01$; a representative experiment is shown in Fig. 2b). Since the ACh binding curve shows little or no GTP-shift under the conditions used (Lu and Hulme, 1999), it is possible that the flattening of the binding curve reflects negative cooperativity between the elements of a dimeric receptor. Analysis using a dimeric receptor model (experimental procedures) provided estimates of 9.57×10^4 M^{-1} and 3.83×10^4 M^{-1} for the mean intrinsic affinity constants of the protomers of the wild type receptor for ACh, with a negative cooperativity of 2.5-fold. Because this is quite small, and because the *pK* values obtained from Hill analysis are very close to the mean

Molecular Pharmacology Fast Forward. Published on September 11, 2007 as DOI: 10.1124/mol.107.038265
This article has not been copyedited and formatted. The final version may differ from this version.

of the *pK* values from the dimeric receptor analysis, the results presented are derived from fits using the Hill equation. Full details are given in supplementary Table 2.

Amongst the ECL2 residues only mutations of Arg171 and Ile180 decreased the affinity of ACh, by 3-4 fold (Fig. 1c).The effect of R171A agrees with published data (Matsui *et al.*, 1995). We did not see a significant effect of F182A on ACh affinity, although an 8-fold reduction in carbachol affinity has been recently reported for the homologous mutation in the M_3 mAChR (Scarselli et al, 2007). The Hill coefficients of the ACh binding curves were unaffected. Single and double substitutions of Cys98 and Cys178 decreased the mean apparent affinity of ACh by 25-70-fold (Fig. 1c). Overall, the means of the Hill coefficients estimated for the C178A and C98A/C178A mutants were not significantly different from 1.0, although a degree of flattening was observed for the C178A mutant in a few experiments (Fig. 2b). However, the mean Hill coefficient for ACh binding to the C98A mutant decreased relative to the wild-type to a mean value of 0.42 ± 0.17 (n=6), significantly different to the wild-type values ($P<0.01$). In favourable cases, it was possible to resolve the binding curve into a predominant low and a residual high affinity population (Fig. 2b). Equally, it was possible to fit the binding curve to a dimeric receptor model (Fig. 2b). Further analysis using the dimeric receptor model (Materials and Methods) provided mean intrinsic pK_d estimates of 2.77 ± 0.24 (C98A), 2.92 ± 0.12 (C178A) and 2.83 ± 0.11 (C98A/C178A) for the low affinity components of the dimer, and 4.0 ± 0.27 (C98A), 3.4 ± 0.24 (C178A) and 2.9 ± 0.22 (C98A/C178A) for the corresponding high affinity components. Thus, of these mutants, it was C98A that

Molecular Pharmacology Fast Forward. Published on September 11, 2007 as DOI: 10.1124/mol.107.038265
This article has not been copyedited and formatted. The final version may differ from this version.

reproducibly manifested a high affinity component. Further experiments are needed to examine whether this mutant exhibits an enhanced GTP shift.

Mutation of Asp99 and Trp378 (the latter measured by inhibition of [^{3}H]QNB binding) reduced ACh affinity by 10-fold, but mutation of Phe197 had no significant effect (Fig. 1c). The Hill coefficient of the ACh binding curve was increased to 1.0 by the W378A mutation.

Phosphoinositide turnover response. In addition to the ECL2 loop mutations reported above, we characterised the PhI response of a series of ECL2 loop mutations of residues conserved in the mAChR subtypes that had previously been characterised in the hM_1 receptor subtype at the level of binding (Matsui *et al.*, 1995). Their expression levels were confirmed by both [^{3}H]NMS and [^{3}H]QNB saturation assays (data not shown), and were similar to wild-type as reported previously (Matsui *et al.*, 1995).

Both rat and human wild-type M_1 mAChRs expressed in COS-7 cells elicited robust and indistinguishable PhI responses to stimulation with ACh with EC_{50} values of 10^{-7} M (Fig. 2c). Significant agonist-independent basal activity (ca. 16% of the maximum ACh-stimulated signal) was seen in most experiments relative to mock-transfected controls. This could be inhibited by atropine (data not shown) and was taken into account in the analysis of the data (experimental procedures).

Molecular Pharmacology Fast Forward. Published on September 11, 2007 as DOI: 10.1124/mol.107.038265
This article has not been copyedited and formatted. The final version may differ from this version.

The mutant receptors exhibited alterations in basal signaling, the potency of ACh, and the E_{max} of the PhI response. The full set of results is summarised in supplementary Table 3. These parameters depend on the expression level of the mutant receptor; the potency is also proportional to the affinity constant of ACh. To compensate for these dependences we calculated a parameter designed to estimate the efficacy of the ACh-receptor complex for initiating a PhI signal (Lu and Hulme, 1999). The results are plotted in Fig. 3, which also shows the amino acid sequence of ECL2, and the probable positioning of the outer (β1) and inner (β2) elements of the modelled anti-parallel β hairpin.

Of the ECL2 loop mutations whose binding properties are reported above, R171A, Q177A and I180A reduced the signaling potency of ACh by 5-fold. Of the additional residues studied, Q165A and G169A gave 3-fold, and W164A and S184A caused 15-30-fold reductions. None of these mutations reduced the maximum PhI response, but W164A, G169A and S184A showed diminished ACh-independent basal signaling activity. Calculations showed that the mutation of a subset of these residues, namely Trp164, Gln177, and Ser184 decreased the ACh signaling efficacy by up to 10-fold, (Figure 3a). In the case of Q181A, the small reduction in calculated signaling efficacy relies on the reported increase in ACh affinity for this mutant (Matsui *et al.*, 1995).

The single and double mutations of Cys98 and Cys178 all diminished the potency of the ACh-induced PhI response by 3000-fold (a representative experiment is shown in Fig. 2c). In contrast to the other ECL2 point mutants, mutations of the Cys residues significantly reduced the maximum ACh-induced signal as well as the agonist-

Molecular Pharmacology Fast Forward. Published on September 11, 2007 as DOI: 10.1124/mol.107.038265
This article has not been copyedited and formatted. The final version may differ from this version.

independent basal signal (Fig. 2c). The cysteine mutations all caused large, 30-60-fold, reductions in the calculated ACh signaling efficacy (Fig. 3a,b).

The D99A mutation reduced the potency of ACh by 100-fold, but did not reduce the calculated signaling efficacy of ACh (Fig.3b), the reduction in PhI potency being attributable to a combination of reduced ACh affinity and receptor expression (Fig. 1a,c).

Ala-substitution of the trans-membrane domain residues Phe197 and Trp378 reduced ACh potency by 30 and 300-fold. The W378A mutation also abolished agonist-independent basal signaling. Calculations indicated that because the F197A mutant showed reduced expression level (Fig. 1a), the reduction in signaling efficacy was only 4-fold (Fig. 3b). In contrast, the effect of W378A was 60-fold.

Radioligand dissociation rate constants. The measurement of dissociation time courses can provide information about the transition from the bound to the free state of the radioligand. Comparison of the dissociation rate constants with the equilibrium binding constants generates additional insight into the role of particular amino acid side-chains in this process.

Wild-type and mutant receptors were labelled to equilibrium with a concentration of [^{3}H]NMS (2×10^{-9} M) or [^{3}H]QNB (2×10^{-10} M) sufficient to give 30% or higher receptor occupancy. Dissociation was started by a 10-fold dilution into 10^{-5} M unlablelled

Molecular Pharmacology Fast Forward. Published on September 11, 2007 as DOI: 10.1124/mol.107.038265
This article has not been copyedited and formatted. The final version may differ from this version.

NMS. The full results are given in supplementary Table 4. A graphical summary is also used in Fig. 8.

[^{3}H]NMS dissociated from the wild-type receptor with a mono-exponential time course corresponding to a half-time of 10.5 minutes (a representative experiment is shown in Fig. 4a) in good agreement with published values (Matsui *et al.*, 1995). The ECL2 loop mutations R171A, I180A and F182A accelerated the dissociation rate of [^{3}H]-NMS by about 2.5-fold, as did C98A (5-fold) and C178A (2.4-fold) (Fig. 4a). In contrast the E170A, Y179A and D99A mutations did not significantly affect the dissociation rate constant of [^{3}H]NMS.

The dissociation of [^{3}H]QNB from the wild-type receptor was much slower, with a mean half-time of approximately 530 minutes. It was also mono-exponential. Y179A and R171A increased the dissociation rate by 3 and 10-fold respectively (Fig. 4b). The C98A and C178A mutations greatly accelerated the dissociation of [^{3}H]-QNB. In the case of C178A, approximately 75 % of the radioligand dissociated in 5 min (Fig. 4c), yielding a 100-fold or greater increase in the rate constant. A small fraction (< 20 %) of a second slower process was seen in 2 out of 3 experiments. In the case of C98A, a bi-exponential process was regularly observed (Fig. 4c), a fast phase (about 50 % of the total) similar to that of C178A, and a second slower phase (k_{off} = 3.07 ± 1 x 10^{-3} min^{-1}; $t_{1/2}$= 225 min) more like the wild-type. Because of the low levels of radioligand binding and rapid dissociation kinetics of the C98A and C178A mutants, it was not possible to determine the rate constants of the fast phase of dissociation precisely.

Molecular Pharmacology Fast Forward. Published on September 11, 2007 as DOI: 10.1124/mol.107.038265
This article has not been copyedited and formatted. The final version may differ from this version.

The D99A mutation did not affect the dissociation rate of [^{3}H]QNB, but the F197A and W378A mutations accelerated it by 10 and 38-fold, respectively; the dissociation time-courses were mono-exponential.

Molecular modelling. Mutations of ligand binding domain residues in TM domains 3 and 4 have been reported to cause mainly parallel reductions in the affinities of NMS, QNB and ACh (Lu and Hulme, 1999). In contrast, some mutations in TM domains 5, 6 and 7 have differential effects on their affinities (Allman *et al.*, 2000; Lu *et al.*, 2001; Ward *et al.*, 1999), as exemplified by F197A in the present study. Some of the key observations are collated in supplementary Table 5.

An optimised rhodopsin-based homology model of the M_1 mAChR has been used to dock ACh, (-)-NMS and (-)-QNB in a manner compatible with the effects of the TM domain Ala-mutations on binding affinity (See Materials and Methods). In attempting to build suitable models, we have prioritised residues whose Ala-substitution caused large (10-fold or greater) reductions in binding affinity, consistent with the participation of their side-chains in direct ligand interactions, and have sought arrangements of these residues that allow them to participate in a coherent binding pocket for the ligand. We have assumed that smaller (less than 10-fold) effects may indicate indirect, or "second shell" effects. However, we recognise that the quantitative effects of Ala-substitution mutations may be modified by factors such as entropy-enthalpy compensation, the displacement of bound water molecules, the deletion of unfavourable interactions, or the

Molecular Pharmacology Fast Forward. Published on September 11, 2007 as DOI: 10.1124/mol.107.038265
This article has not been copyedited and formatted. The final version may differ from this version.

development of compensating interactions, for instance by the substitution of a solvent molecule for the deleted side-chain.

The results of the docking experiments are represented in Figures 5 and 6. The positively-charged quaternary ammonium head-groups of ACh and NMS form an ion-pair with the carboxylate group of Asp105 (TM3). The tertiary nitrogen on the quinuclidine ring system of QNB has a pKb of 8.69 (ACD pKa calculator) and is protonated under physiological conditions, also allowing it to form an ionic interaction with Asp 105.

This interaction is reinforced by contacts of neighbouring residues, particularly Tyr106, H-bonded to the carbonyl group of ACh, contacting the scopine ring of NMS, and the quinuclidine ring and ester oxygen, as well as one of the phenyl rings of QNB. Trp378 contributes to the floor of the binding site in all three cases. Thus, the head-groups of these ligands occupy overlapping spaces within the binding pocket. Furthermore, the proximal parts of the side-chains all make contact with Asn382, potentially reinforced, in the case of NMS, by a hydrogen bond between the hydroxyl-methyl group of the tropic acid moiety of NMS and the amide group.

In contrast, the positions of the side-chain termini are different. The phenyl ring of the tropic acid side-chain of NMS is modelled as projecting into the trans-membrane domain past Ala193 towards the ring of Phe197. The mutation A193G has been reported to decrease NMS affinity (Allman *et al.*, 2000). The shorter side-chain of ACh does not reach so far into the trans-membrane domain, instead projecting towards TM5 at a level

Molecular Pharmacology Fast Forward. Published on September 11, 2007 as DOI: 10.1124/mol.107.038265
This article has not been copyedited and formatted. The final version may differ from this version.

slightly below Thr189, the mutation of which decreases ACh affinity (Allman *et al.*, 2000). In contrast, the two phenyl rings of the benzilyl moiety of QNB are modelled in a more superficial position in the binding site, interacting with Tyr106 and Trp157, and Asn382 respectively. Such additional side-chain interactions may account for the enhanced affinity of QNB with respect to NMS, diminishing the relative importance of Tyr381 (TM6), whose mutation strongly decreases the affinities of NMS and ACh, but not QNB (Ward *et al.*, 1999).

Calculations of the energy of interaction between the ligands and individual side-chains in the receptor model (Materials and Methods) are qualitatively consistent with the mutagenesis data. The energies calculated by the energy de-convolution are the summed steric and electrostatic contributions from the residues interacting with the ligand. A caveat is that Ala substitution-induced changes in ligand binding affinity are not necessarily a direct measure of side-chain interaction energies, and do not address the contribution of the polypeptide backbone and the β-carbon.

The plots shown in Fig. 7 compare the two data sets on a normalised scale. They emphasise the primary importance of interactions at the level of Asp105 and Tyr106 in TM3, and Trp378, Tyr381 and Asn382 in TM6 for the binding of all three ligands. By comparison with the Ala-substitution data, there is apparent over-emphasis of the importance of the ionic interaction with Asp105 for the binding of ACh and NMS. The calculated contributions of Trp378, Tyr381, Asn382 and Val385 to the binding of ACh and NMS follow the mutagenesis data reasonably well. In the case of QNB, the

Molecular Pharmacology Fast Forward. Published on September 11, 2007 as DOI: 10.1124/mol.107.038265
This article has not been copyedited and formatted. The final version may differ from this version.

contribution of Tyr381 is predicted to be less than that of Asn382, but the experimental difference is more pronounced, because the Y381A mutation has remarkably little effect on the affinity of QNB (Ward *et al.*, 1999), while for V385, the β-carbon makes the predominant contribution to the calculated energy of QNB binding and this is preserved in the Ala-mutant. In TM7, the model suggests that Y404 contributes to NMS and ACh but not QNB binding, in agreement with the mutagenesis data.

The selective importance of Phe197 for the binding of NMS is reproduced in the energy calculations. The substantial distance between the ligands and residues in ECL2, including Cys178, is also reflected in the low calculated interaction energies, although Tyr179 is predicted to make some contribution to the binding energy of ACh and QNB, but not NMS. In fact, the Y179A mutation significantly accelerated the dissociation rate of QNB (Fig. 4b) but not NMS, and did not affect the equilibrium affinity constant of ACh. At the top of TM3, Cys98 and Asp99 are also not predicted to make much contribution to ligand binding energy. We have not attempted to model the more global conformational changes that might be expected to result from the mobilisation of ECL2 after mutagenic disruption of the disulfide bond. These may underlie the substantial effects of these mutations on ligand binding affinities.

The role of Trp157 deserves comment. In a previous model of the M_1 mAChR the ring of Trp157 was modelled as projecting towards the outer surface of the receptor (Lu *et al.*, 2001). To account for the important effect of the W157A mutation on the affinities of all three ligands, we have instead modelled the indole ring of Trp157 as projecting inward

toward the binding cavity, where it can form a parallel stacking interaction with the phenyl ring of Tyr106. This energetically-favourable conformation may help to stabilise the contributions of Tyr106 to ACh and NMS binding, in addition to any direct contributions that the indole ring of Trp157 may make. In the QNB complex, the stacking interaction is relaxed to incorporate one of the two phenyl rings of QNB. This re-orientation of the side-chain of Trp157 enables it to make a small direct contribution to ligand binding energy although this is still not large enough to account for the effect of the W157A mutation.

Molecular Pharmacology Fast Forward. Published on September 11, 2007 as DOI: 10.1124/mol.107.038265
This article has not been copyedited and formatted. The final version may differ from this version.

Discussion

The Ala-substitutions of individual ECL2 residues reduced the affinities of the antagonist NMS and the agonist ACh by less than 5-fold, and did not alter the affinity of QNB. Taking published results into account (Matsui *et al.*, 1995; Gnagey *et al.*, 1999; Scarselli *et al.*, 2007), 18 of the 22 non-disulfide bonded residues of ECL2 of the mAChRs have been mutated without identifying a candidate primary contact residue for orthosteric ligands. The sequence positions that showed reduced NMS affinity are homologous to retinal contact residues in rhodopsin, but in the M_1 mAChR these amino acids may be in the "second shell", shaping the environment of the binding site without making primary ligand contacts. This view is consistent with molecular models of the binding site.

Mutations of Trp164, Gln181 and Ser184 (fully-conserved in the mammalian mAChR subtypes) and Gln177 (found in M_1 and M_4 becoming Glu in M_2, M_3 and M_5) reduced the calculated ACh signaling efficacy by up to 10-fold. Excepting Gln181, these positions were not picked up in a recent random mutagenesis and Ala-substitution study of the M_3 mAChR where carbachol was used as the activating ligand (Scarselli *et al.*, 2007). Although noticeable, these effects are not as large as the 100-1000-fold reductions following mutations of key residues in the TM domain (Lu *et al.*, 2001). Several corresponding residues in rhodopsin (M_1 mAChR equivalent in brackets) namely Trp175 (Trp164), Asp190 (Gln181) and Thr193 (Ser184) participate in hydrogen-bond networks to the adjacent TM helices 4 and 5 (Li *et al.*, 2004). Plausibly, the corresponding M_1

Molecular Pharmacology Fast Forward. Published on September 11, 2007 as DOI: 10.1124/mol.107.038265
This article has not been copyedited and formatted. The final version may differ from this version.

mAChR residues may have a similar role in micro-domains linking ECL2 to the TM domain. In contrast to a recent study on the C5a receptor (Klco *et al.*, 2005), none of the Ala-substitutions caused reproducible constitutive activity.

Single and double mutations of Cys178 and Cys98 strongly reduced receptor expression levels underlining the importance of these highly conserved residues for receptor folding and cell-surface expression. Nevertheless, an atropine-rescue protocol enabled us to characterise their properties.

The mutations caused 10-20-fold reductions in the affinities of NMS and QNB, less than initially reported for the M_3 receptor (Zeng *et al.*, 1999) but comparable with a very recent study on M_2 and M_3 mAChRs, (Huang and Ellis, 2007), and much smaller than the effect of mutating direct ligand-contact residues (Ward *et al.*, 1999). The non-additivity is consistent with the disulfide bond between Cys98 and Cys178. The homogeneity of the effects of C98A, C178A and Cys178N on the affinities of NMS and QNB argues that the Cys residues do not contribute directly to the binding of either of these antagonists. More likely, the reduced affinity reflects general destabilisation of the trans-membrane binding pocket following scission of the link between TM3 and 5.

The mutations of Cys98 and Cys178 caused larger, 80-fold, reductions in ACh affinity, as seen for primary binding site residues such as Asp105 (Lu and Hulme, 1999). However, in TM3, mutation of residues one helical turn above and below Asp105 reduced ACh affinity 30-fold, but there were no large effects of mutating neighbouring

residues in ECL2, and no differential effects of the C178N and C178A mutations. Therefore the reduction in ACh affinity also probably reflects a global disturbance of the trans-membrane binding pocket consequent on weakening the constraints between the tops of TM domains 3 and 5, both of which harbour residues important for the binding of ACh (Allman *et al.*, 2000). The solvent network within the binding pocket, that influences the thermodynamics of ACh binding (Hulme *et al.*, 2006), may also be strongly perturbed. The cumulative effects may explain the 60-fold reduction in ACh signaling efficacy.

For C98A, the residual population of high-affinity ACh binding sites observed in membrane binding studies may explain the biphasic [^{3}H]QNB dissociation curve. These sites, if present in whole cells, cannot be functional in signaling because their apparent affinity for ACh exceeds the ACh potency for the PhI response. The free Cys178 sulfhydryl may be able to form a non-natural disulfide bond (Noda *et al.*, 1994) or promote the formation of disulfide-linked oligomers (Zeng and Wess, 1999).

The D99A mutation reduced the affinity of ACh and NMS 10-fold without affecting the affinity of QNB, or changing the computed signaling efficacy of ACh. These findings are consistent with the effect of the D99N mutation (Fraser *et al.*, 1989). They contrast sharply with the effect of mutating Asp105 which strongly reduced QNB affinity, and abolished ACh signaling (Lu and Hulme, 1999; Fraser *et al.*, 1989).

Molecular Pharmacology Fast Forward. Published on September 11, 2007 as DOI: 10.1124/mol.107.038265
This article has not been copyedited and formatted. The final version may differ from this version.

A comparison of the mutation-induced changes in the dissociation rate constants with the binding constants of NMS provided further insight (Fig. 8a). The substitution of side-chains which make a favourable contribution to the free energy of the ligand in the receptor binding site should decrease the affinity constant and the free energy barrier of the reverse (dissociation) reaction to equal extents as reported for Y404A (7.39) (Matsui *et al.*, 1995). Although the effects were small, the predicted correlation was shown by the ECL2 point mutants that exhibited reduced NMS affinity (with the possible exception of Y179A).

In contrast, for the mutations of Asp99 and the disulfide-bonded Cys residues the increases in the dissociation rate constant were insufficient to account for the decreases in NMS affinity. Thus their primary effect may be to decrease the association rate constant for NMS binding. Similar effects followed Ala mutations of tryptophan residues in ECL1 and at the tops of TM3 and TM7 (Matsui *et al.*, 1995). Structures created by the disulfide link between Cys98 and Cys178 as well as individual residues such as Asp99 may contribute to a channel that allows hydrophilic ligands such as NMS to access the transmembrane binding pocket. Asp99 may be a “gatekeeper” residue to the entrance channel for positively-charged ligands. This may resemble the entrance channel in acetylcholine esterase (Koellner *et al.*, 2000).

The lipophilic tertiary amine QNB gave a different picture (Fig. 8b). Ala-substitution of Asp99 did not increase its dissociation rate. However mutation of Cys98 and Cys178 induced a fast phase of QNB dissociation. This was accelerated beyond the expectation

from the decrease in the affinity constant. Mutation of Arg171 also selectively accelerated QNB dissociation. Calculated from the product of the affinity constant and the dissociation rate constant, the association rate constant of QNB for the wild-type receptor was 5.7 x 10^5 $M^{-1}s^{-1}$, about 10 % of the value of 7.3 x 10^6 $M^{-1}s^{-1}$ for NMS, in agreement with published estimates (Waelbroeck *et al.*, 1991). Compared to NMS, the access of the bulkier hydrophobic QNB to the wild-type receptor binding site is selectively hindered. QNB may not pass through a restrictive hydrophilic channel as readily as NMS. However, mutation of the disulfide-bonded Cys residues, or of Arg171, increased the calculated association rate constant of QNB up to 10-fold. These mutations may destabilise the structure of the receptor, amplifying breathing motions that facilitate the access of QNB to the binding site by an alternative route. Structural destabilisation, detected by accelerated dissociation of QNB, may also follow the mutation of well-packed residues such as Phe197 and Trp378 in the TM domain.

At the bottom of the binding pocket, mutagenesis and modelling suggest that Trp378 (6.48) contributes directly to the binding pocket for NMS, QNB and ACh, although possibly with different side-chain orientations. In the M_3 mAChR, the mutation of Trp 6.48 to Phe reduced NMS affinity by only 5-fold but ACh affinity by 18-fold (Wess *et al.*, 1993). Thus, the aromatic character of Trp378 may be key for the binding of NMS, but less important for the ground-state binding of ACh as found for Tyr381 (6.51) (Ward *et al.*, 1999). Trp378, like Tyr381, is crucial for receptor signaling, suggesting that both of the aromatic residues bracketing the kink-inducing Pro380 (6.50) may develop enhanced interactions with ACh in the activated state of the receptor.

Molecular Pharmacology Fast Forward. Published on September 11, 2007 as DOI: 10.1124/mol.107.038265
This article has not been copyedited and formatted. The final version may differ from this version.

In marked contrast, the F197A mutation reduced the affinity of NMS 40-fold without affecting QNB or ACh affinity. To achieve consistency, molecular modelling studies suggest that the side-chains of NMS and QNB follow distinct vectors within the binding site (Fig. 5). The phenyl ring of the tropic acid side-chain of NMS may extend deep into the trans-membrane region towards TM5 while the bulkier benzilate group of QNB is retained at the top of the binding pocket, interacting with the upper parts of TM3, 4 and 6. This docking posture is consistent with the lack of effect of mutations in TM7 on QNB affinity (Lu *et al.*, 2001). It differs from a recent ab-initio modelling prediction (Peng *et al.*, 2006). Dissimilar docking of NMS and QNB might affect not only the kinetics of formation and breakdown but also the functional properties of the receptor-ligand complexes, perhaps accounting for differences in cooperativity between NMS, QNB and allosteric ligands (Lanzafame *et al.*, 2006) and affecting the potential for inverse agonism (Schwartz *et al.*, 2006). The shorter side-chain of ACh also fails to penetrate far into the TM domain, and is unlikely to interact strongly with TM5 in the ground state of the receptor.

Molecular Pharmacology Fast Forward. Published on September 11, 2007 as DOI: 10.1124/mol.107.038265
This article has not been copyedited and formatted. The final version may differ from this version.

Acknowledgements

The authors are grateful to Dr. Nigel Birdsall (National Institute for Medical Research, U.K.) for the gift of mutations in ECL2 and for helpful comments on the manuscript.

Molecular Pharmacology Fast Forward. Published on September 11, 2007 as DOI: 10.1124/mol.107.038265
This article has not been copyedited and formatted. The final version may differ from this version.

Reference List

Allman K, Page K M, Curtis C A M and Hulme E C (2000) Scanning mutagenesis identifies amino acid side chains in transmembrane domain 5 of the M_1 muscarinic receptor that participate in binding the acetyl methyl group of acetylcholine. *Mol Pharmacol* **58**:175-184.

Azpiazu I and Gautam N (2004) A fluorescence resonance energy transfer-based sensor indicates that receptor access to a G protein is unrestricted in a living mammalian cell. *J Biol Chem* **279**:27709-27718.

Ballesteros JA and Weinstein H (1995) Integrated methods for the construction of three dimensional models and computational probing of structure-function relations in G-protein-coupled receptors. *Methods Neurosci* **25**:366-428.

Blaney, F. E. Approaches to the molecular modelling of 7-transmembrane helical receptors. [9], 8.1-8.41. 2006. John Wiley and Sons Inc. Current Protocols in Pharmacology.

Blaney FE, Raveglia L F, Artico M, Cavagnera S, Dartois C, Farina C, Grugni M, Gagliardi S, Luttmann M A, Martinelli M, Nadler G M, Parini C, Petrillo P, Sarau H M, Scheideler M A, Hay D W and Giardina G A (2001) Stepwise modulation of neurokinin-3 and neurokinin-2 receptor affinity and selectivity in quinoline tachykinin receptor antagonists. *J Med Chem* **44**:1675-1689.

Bourdon H, Trumpp-Kallmeyer S, Schreuder H, Hoflack J, Hibert M and Wermuth C G (1997) Modelling of the binding site of the human m1 muscarinic receptor: experimental validation and refinement. *J Comput Aided Mol Des* **11**:317-332.

Dunbrack RL and Karplus M (1993) Backbone-dependent rotamer library for proteins. Application to side-chain prediction. *J Mol Biol* **230**:543-574.

Fraser CM, Wang C-D, Robinson D A, Gocayne J D and Venter J C (1989) Site-directed mutagenesis of m_1 muscarinic acetylcholine receptors: Conserved aspartic acids play important roles in receptor function. *Mol Pharmacol* **36**:840-847.

Gnagey AL, Seidenberg M and Ellis J (1999) Site-directed mutagenesis reveals two epitopes involved in the subtype selectivity of the allosteric interactions of gallamine at muscarinic acetylcholine receptors. *Mol Pharmacol* **56**:1245-1253.

Heitz F, Holzwarth J A, Gies J-P, Pruss R M, Trumpp-Kallmeyer S, Hibert M and Guenet C (1999) Site-directed mutagenesis of the putative human muscarinic M_2 receptor binding site. *Eur J Pharmacol* **380**:183-105.

Huang XP and Ellis J (2007) Mutational disruption of a conserved disulfide bond in muscarinic acetylcholine receptors attenuates positive homotropic cooperativity between multiple allosteric sites and has subtype-dependent effects on the affinities of muscarinic allosteric ligands. *Mol Pharmacol* **71**:759-768.

Hulme EC (2006) Systematic mutagenesis of M1 muscarinic acetylcholine receptors, in *G Protein-Coupled Receptors* (Haga T and Takeda S eds) pp 137-178, CRC Press, Boca Raton, Florida.

Hulme EC, Lu Z L and Bee M S (2003) Scanning mutagenesis studies of the M-1 muscarinic acetylcholine receptor. *Receptors & Channels* **9**:215-228.

Hulme EC, Soper A K, McLain S E and Finney J L (2006) The hydration of the neurotransmitter acetylcholine in aqueous solution. *Biophys J* **91**:2371-2380.

Jones PG, Curtis C A and Hulme E C (1995) The function of a highly-conserved arginine residue in activation of the muscarinic M1 receptor. *Eur J Pharmacol* **288**:251-257.

Klco JM, Wiegand C B, Narzinski K and Baranski T J (2005) Essential role for the second extracellular loop in C5a receptor activation. *Nat Struct Mol Biol* **12**:320-326.

Kniazeff J, Bessis A S, Maurel D, Ansanay H, Prezeau L and Pin J P (2004) Closed state of both binding domains of homodimeric mGlu receptors is required for full activity. *Nat Struct Mol Biol* **11**:706-713.

Koellner G, Kryger G, Millard C B, Silman I, Sussman J L and Steiner T (2000) Active-site gorge and buried water molecules in crystal structures of acetylcholinesterase from Torpedo californica. *J Mol Biol* **296**:713-735.

Kurtenbach E, Curtis C A M, Pedder E K, AitkenA, Harris A C M and Hulme E C (1990) Muscarinic acetylcholine receptors: Peptide sequenceing identifies residues involved in antagonist binding and disulfide bond formation. *J Biol Chem* **265**:13702-13708.

Lanzafame AA, Sexton P M and Christopoulos A (2006) Interaction studies of multiple binding sites on m4 muscarinic acetylcholine receptors. *Mol Pharmacol* **70**:736-746.

Li B, Scarselli M, Knudsen C D, Kim S K, Jacobson K A, McMillin S M and Wess J (2007) Rapid identification of functionally critical amino acids in a G protein-coupled receptor. *Nat Methods* **4**:169-174.

Li J, Edwards P C, Burghammer M, Villa C and Schertler G F (2004) Structure of bovine rhodopsin in a trigonal crystal form. *J Mol Biol* **343**:1409-1438.

Lu Z-L, Saldanha J and Hulme E C (2001) Transmembrane domains 4 and 7 of the M_1 muscarinic acetylcholine receptor are critical for ligand binding and the receptor activation switch. *J Biol Chem* **276**:34098-34104.

Lu Z-L, Curtis C A M, Jones P G, Pavia J and Hulme E C (1997) The Role of the Aspartate-Arginine-Tyrosine Triad in the m1 Muscarinic Receptor: Mutations of aspartate 122 and tyrosine 124 decrease receptor expression but do not abolish signaling. *Mol Pharmacol* **51**:234-241.

Lu Z-L and Hulme E C (1999) The functional topography of transmembrane domain 3 of the M1 muscarinic acetylcholine receptor, revealed by scanning mutagenesis. *J Biol Chem* **274**:7309-7315.

Ludeke S, Beck M, Yan E C, Sakmar T P, Siebert F and Vogel R (2005) The role of Glu181 in the photoactivation of rhodopsin. *J Mol Biol* **353**:345-356.

Matsui H, Lazareno S and Birdsall N J M (1995) Probing of the location of the allosteric site on m1 muscarinic receptors by site-directed mutagenesis. *Mol Pharmacol* **47**:88-98.

Noda K, Saad Y, Graham R M and Karnik S S (1994) The high affinity state of the β_2-adrenergic receptor requires unique interaction between conserved and non-conserved extracellular loop cysteines. *J Biol Chem* **269**:6743-6752.

Palczewski K, Kumasaka T, Hori T, Behnke C A, Motoshima H, Fox B A, Le Trong I, Teller D C, Okada T, Stenkamp R E, Yamamoto M and Miyano M (2000) Crystal structure of rhodopsin: A G protein-coupled receptor. *Science* **289**:739-745.

Peng JY, Vaidehi N, Hall S E and Goddard W A, III (2006) The Predicted 3D Structures of the Human M1 Muscarinic Acetylcholine Receptor with Agonist or Antagonist Bound. *ChemMedChem* **1**:878-890.

Savarese TM, Wang C-D and Fraser C M (1992) Site-directed mutagenesis of the rat m1 muscarinic acetylcholine receptor: role of conserved cysteines in receptor function. *J Biol Chem* **267**:11439-11448.

Scarselli M, Li B, Kim S K and Wess J (2007) Multiple residues in the second extracellular loop are critical for M3 muscarinic acetylcholine receptor activation. *J Biol Chem* **282**:7385-7396.

Schwartz TW, Frimurer T M, Holst B, Rosenkilde M M and Elling C E (2006) Molecular mechanism of 7TM receptor activation--a global toggle switch model. *Annu Rev Pharmacol Toxicol* **46**:481-519.

Terakita A, Koyanagi M, Tsukamoto H, Yamashita T, Miyata T and Shichida Y (2004) Counterion displacement in the molecular evolution of the rhodopsin family. *Nat Struct Mol Biol* **11**:284-289.

Waelbroeck M, Tastenoy M, Camus J and Christophe J (1991) Binding kinetics of quinuclidinyl benzilate and methyl-quinuclidinyl benzilate enantiomers at neuronal (M1), cardiac (M2), and pancreatic (M3) muscarinic receptors. *Mol Pharmacol* **40**:413-420.

Ward SDC, Curtis C A M and Hulme E C (1999) Alanine-scanning mutagenesis of transmembrane domain 6 of the M_1 muscarinic acetylcholine receptor suggests that Tyr381 plays key roles in receptor function. *Mol Pharmacol* **56**:1031-1041.

Wess J (1996) Molecular biology of muscarinic acetylcholine receptors. [Review] [196 refs]. *Crit Rev Neurobiol* **10**:69-99.

Wess J, Nanavati S, Vogel Z and Maggio R (1993) Functional role of proline and tryptophan residues highly conserved among G protein-coupled receptors studied by mutational analysis of the m3 muscarinic receptor. *The EMBO Journal* **12**:331-338.

Zeng F-Y, Soldner A, Schoneberg T and Wess J (1999) Conserved extracellular cysteine pair in the M3 muscarinic acetylcholine receptor is essential for proper receptor cell surface localization but not G protein coupling. *J Neurochem* **72**:2404-2414.

Zeng F-Y and Wess J (1999) Identification and molecular characterisation of m3 muscarinic receptor dimers. *J Biol Chem* **274**:19487-19497.

Molecular Pharmacology Fast Forward. Published on September 11, 2007 as DOI: 10.1124/mol.107.038265
This article has not been copyedited and formatted. The final version may differ from this version.

Footnotes

Alex Goodwin was supported by a Medical Research Council post-graduate studentship.

This work was supported by the Medical Research Council, U.K.

Reprint requests to

E.C. Hulme, Ph.D.,

Division of Physical Biochemistry,

MRC National Institute for Medical Research,

The Ridgeway,

Mill Hill,

London NW7 1AA,

U.K.

ehulme@nimr.mrc.ac.uk

Molecular Pharmacology Fast Forward. Published on September 11, 2007 as DOI: 10.1124/mol.107.038265
This article has not been copyedited and formatted. The final version may differ from this version.

FIGURE LEGENDS

Fig. 1. The effects of alanine-substitution of residues in extracellular loop 2 and in the transmembrane domain on the level of expression and binding affinity of M_1 mAChRs in COS-7 cells. Full details are given in supplementary Tables 1 and 2.

(a) Effects on receptor expression level, calculated from saturation curves with [^{3}H]NMS and [^{3}H]QNB. Bars show the change in expression level relative to contemporaneously-transfected wild-type controls. Except for F197A and W378A, the values show the weighted mean ± SEM of two sets of measurements, one with [^{3}H]NMS and the other with [^{3}H]QNB (n=3-10; supplementary Table 1). Hatched bars indicate mutants where expression was rescued by atropine treatment of the cells after transfection. * $P<0.05$, ** $P<0.01$ with respect to wild-type.

(b) Effects on affinity for NMS and QNB. Changes in affinity relative to wild-type are displayed on a log scale, and represent the mean ± SEM of 3-10 independent measurements. *$P<0.05$, ** $P<0.01$ with respect to wild-type (n=14, [^{3}H]NMS; n=10, [^{3}H]QNB).

Molecular Pharmacology Fast Forward. Published on September 11, 2007 as DOI: 10.1124/mol.107.038265
This article has not been copyedited and formatted. The final version may differ from this version.

(c) Effects on affinity for ACh. Changes in pIC_{50} relative to wild-type are displayed and represent the mean ± SEM of 3-9 independent measurements. *P<0.05; **P<0.01 with respect to wild-type (n=27).

Fig. 2. Representative experiments showing membrane ligand binding and whole cell signaling properties of the wild-type M_1 mAChR (●), C98A (▼), C178A (■) and C98A/C178A (♦) mutants expressed in COS-7 cells.

(a) Inhibition of the specific binding of [^{3}H]NMS ($1.17x10^{-11}$ M, WT; 2.12×10^{-10} M, mutants) by unlabelled NMS. Curves are fits to a 1-site model of binding giving pK_d estimates of: WT, 9.5; C98A, 8.3; C178A, 8.4 and C98A/C178A, 8.2,

(b) Inhibition of the specific binding of [^{3}H]NMS ($1.07x\ 10^{-10}$ M, WT; $1.9\text{-}2.5\ x\ 10^{-9}$ M, mutants) by ACh. Full lines are fits to the Hill equation giving Cheng-Prusoff-corrected pIC_{50} (n_H) estimates of: WT, 4.82 (0.71); C178A 3.29 (0.57); C98A/C178A, 3.00 (1.04), or to a 2-site model of binding giving pK_d values for C98A of 5.75 (37 % of total sites) and 2.28 (63 % of total sites). The dotted line shows the fit of the dimeric receptor model to the C98A data with $pK_{L1} = pK_{L2} = 8.46$, $pK_{L3} = 8.65$, $pK_{A1} = 4.65$, and $pK_{A2} = 2.62$.

(c) ACh-induced [^{3}H]PhI response. Curves are fits to a 4-parameter logistic function giving pEC_{50} values of: WT, 7.3; C98A, 3.75; C178A, 3.51 and C98A/C178A, 3.40 . E_{max} (% WT) values were C98A, 40 %; C178A, 55 % and C98A/C178A, 30 %.

Molecular Pharmacology Fast Forward. Published on September 11, 2007 as DOI: 10.1124/mol.107.038265
This article has not been copyedited and formatted. The final version may differ from this version.

Fig. 3. Plots of mutation-induced changes in signaling efficacy against sequence position. Full details of the effects of the mutations on the PhI signaling response are given in supplementary Table 3. ACh binding affinity and potency in eliciting a PhI response and the receptor expression level were used to calculate the signaling efficacy of the response of each mutant to ACh as described previously (see materials and methods). Bars represent the logs of the signaling efficacy of each mutant relative to the wild-type receptor. Where no bar is shown the value has not been determined. (a) ECL2 mutants; the arrows represent the position of the outer and inner strands of the presumed β-hairpin; (b) TM domain mutants.

Fig. 4 Representative experiments showing dissociation time courses of radioligands from wild-type and mutant M_1 mAChRs. Unless otherwise indicated, curves are fits to single exponentials normalised to the initial level of specific binding. k_{off} values are in units of min^{-1}. Full details are given in supplementary Table 4.

(a) Dissociation of [^{3}H]NMS. k_{off} values are WT, 0.071 (●); D99A, 0.052 (▼); C98A, 0.19 (■) and C178A, 0.14 (♦).

(b) Dissociation of [^{3}H]QNB. k_{off} values are WT, 0.0024 (●); R171A, 0.0242 (▼) and Y179A, 0.0113 (■).

Molecular Pharmacology Fast Forward. Published on September 11, 2007 as DOI: 10.1124/mol.107.038265
This article has not been copyedited and formatted. The final version may differ from this version.

(c) Dissociation of [^{3}H]QNB. k_{off} values are WT, 0.0024 (●); C98A (double-exponential fit) 0.4 (49 % of total) and 0.004 (▼); C178A (double-exponential fit) 0.5 (82 % of total) and 0.019 (■).

Fig. 5. Molecular model of the M_1 mAChR binding site docked with (a) acetylcholine, (b) S-(-)-N-methyl scopolamine and (c) R-(-)-3-quinuclidinyl benzilate.

Fig. 6. 2-dimensional LIGPLOTS, of the modelled M_1 mAChR binding site docked with (a) acetylcholine, (b) S-(-)-N-methyl scopolamine and (c) R-(-)-3-quinuclidinyl benzilate. Hatched semi-circles indicate residues involved in hydrophobic contacts. Dotted lines show hydrogen bonds; for ACh, the indicated H-bond length is 3.32 Å; for QNB it is 2.86 Å.

Fig. 7. Comparison of mutation-induced changes in binding affinity ($\Delta\ pK_d$) with computed contributions of amino acid side-chains to the binding energies for acetylcholine, S-(-)-N-methyl scopolamine and R-(-)-3-quinuclidinyl benzilate on a normalised scale. For plotting, each individual ΔpK_d or deconvoluted energy value was scaled by division by the sum of the corresponding values taken over the following residues: L102, Y106, S109, W157, W378, Y381, N382, Y404, C407, thus for the ith residue the values plotted were $\Delta pK_d^i / \Sigma\Delta pK_{d,\,\mathrm{L102,\,Y106\ldots C407}}$ and $E^i/\Sigma E_{\mathrm{L102,Y106....C407}}$.

Molecular Pharmacology Fast Forward. Published on September 11, 2007 as DOI: 10.1124/mol.107.038265
This article has not been copyedited and formatted. The final version may differ from this version.

Fig. 8. Plots of mutation-induced changes in dissociation rate constant against changes in affinity. Values are represented on a log scale. The full line is the line of equivalence. (a) NMS; (b) QNB.

Molecular Pharmacology Fast Forward. Published on September 11, 2007 as DOI: 10.1124/mol.107.038265
This article has not been copyedited and formatted. The final version may differ from this version.

Figure 1

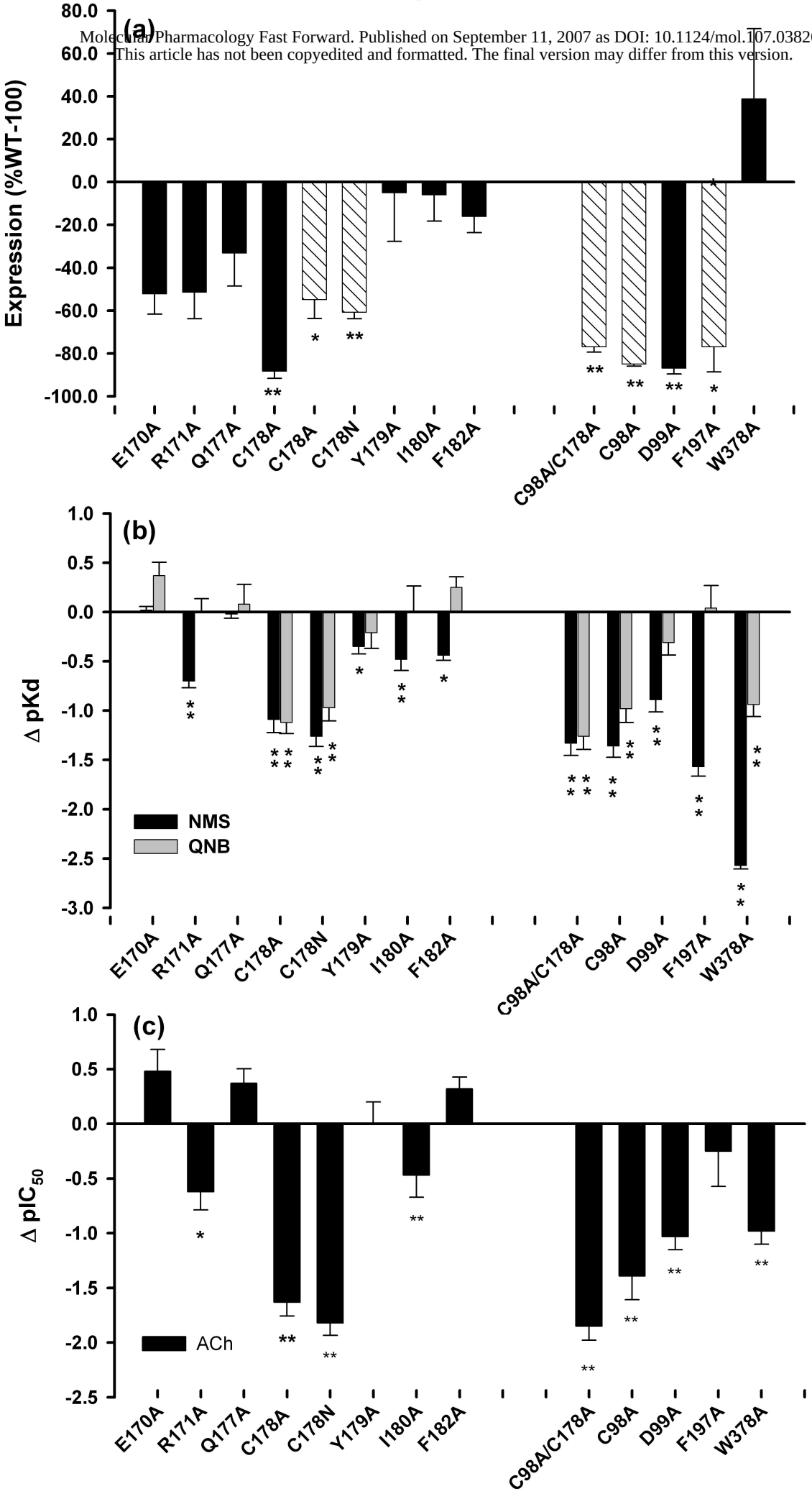

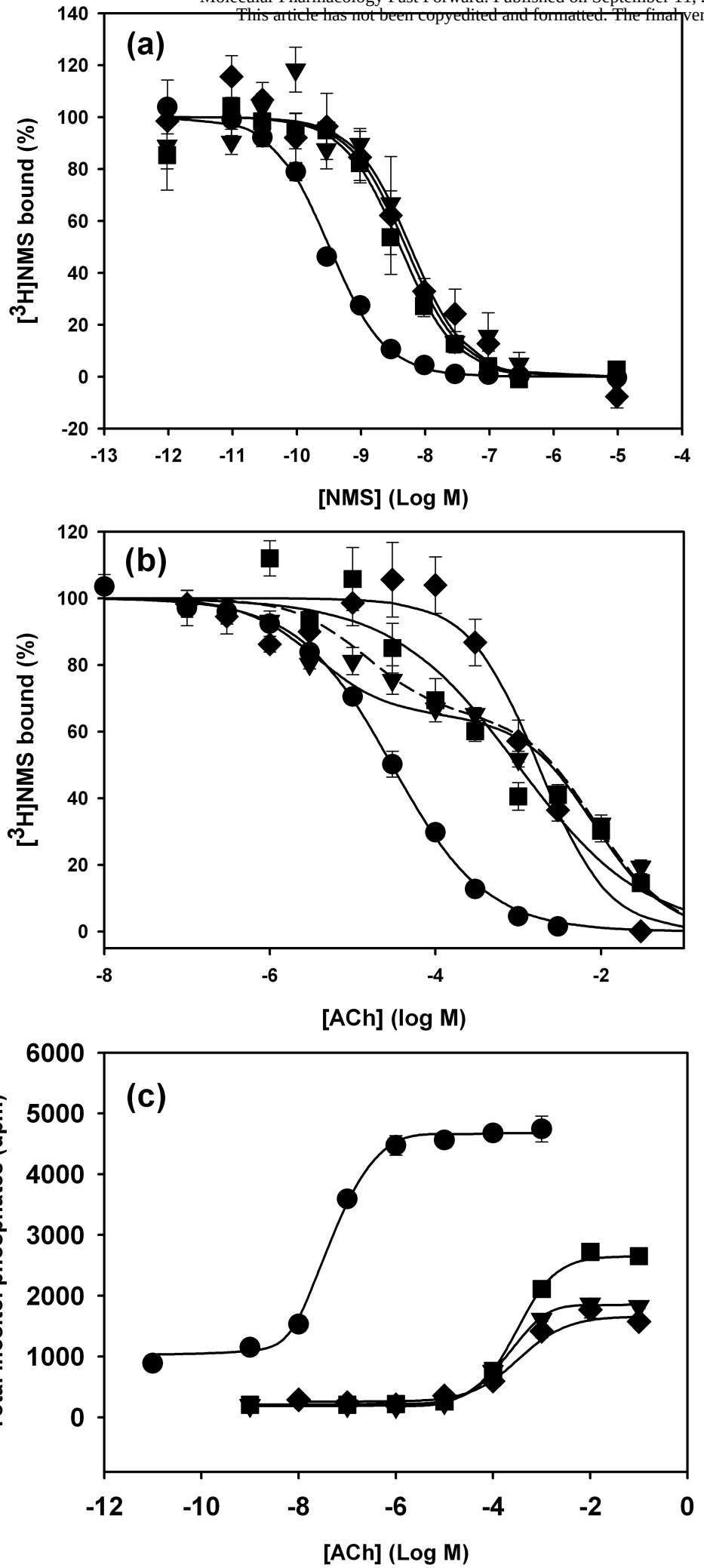

Figure 3

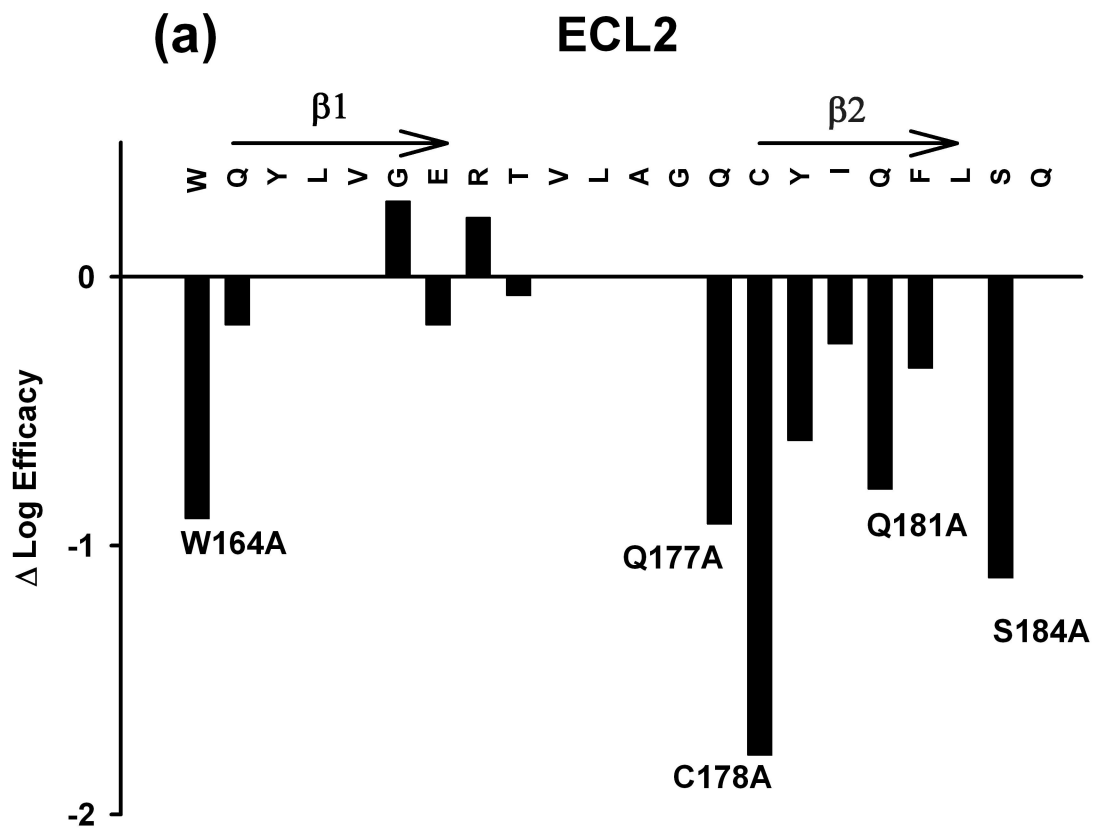
(a)
ECL2
β1
β2
W Q Y L V G E R T V L A G Q C Y I Q F L S Q
0
-1
-2
Δ Log Efficacy
W164A
Q177A
C178A
Q181A
S184A

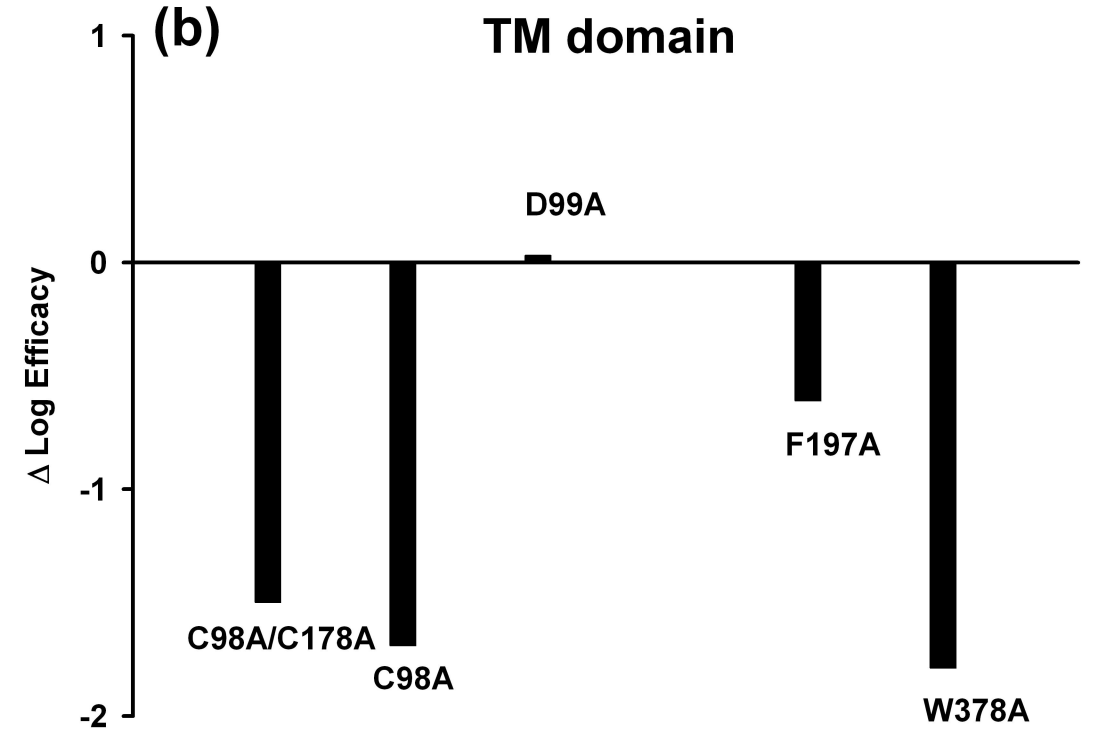
(b)
TM domain
1
0
-1
-2
Δ Log Efficacy
D99A
C98A/C178A
C98A
F197A
W378A

Figure 4

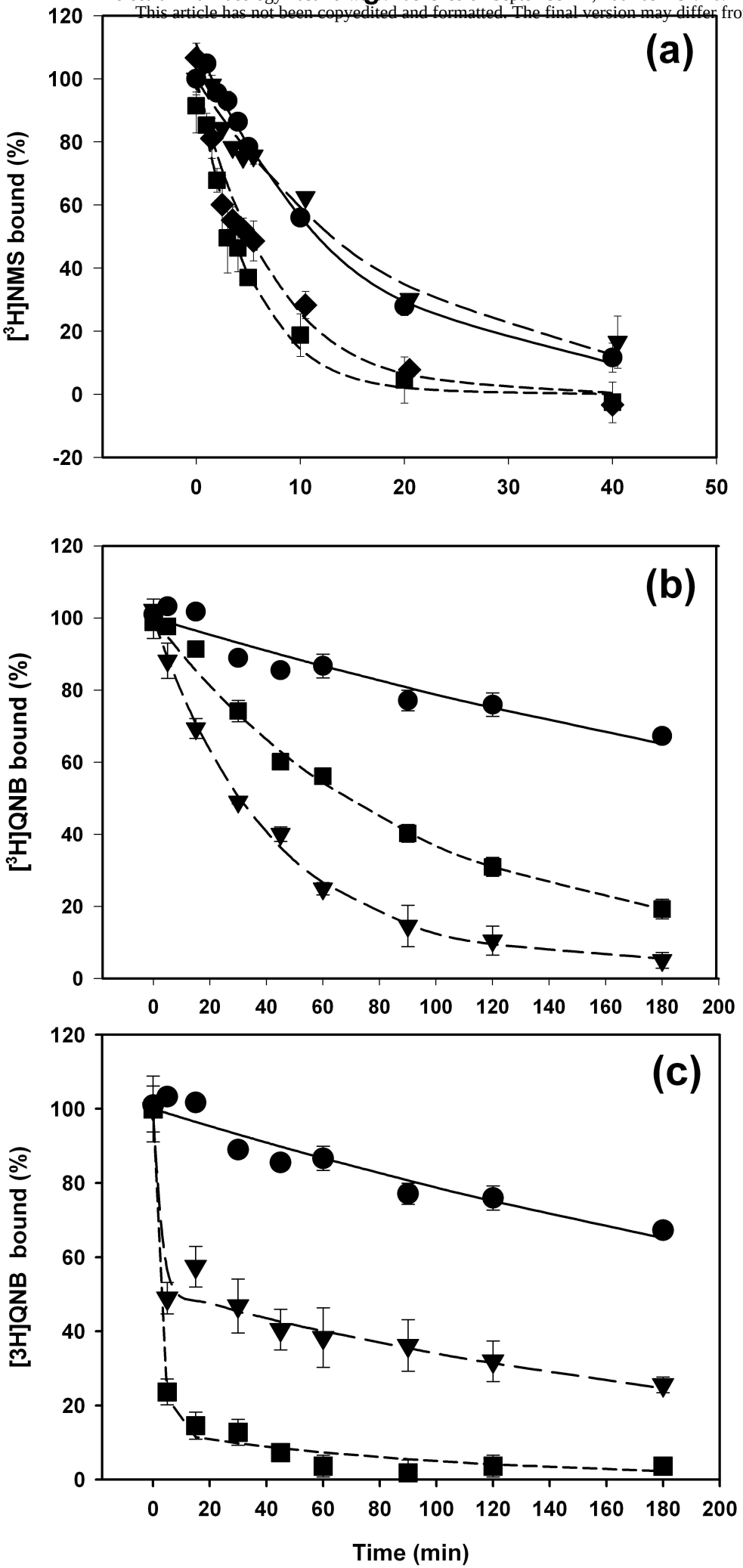

Figure 5

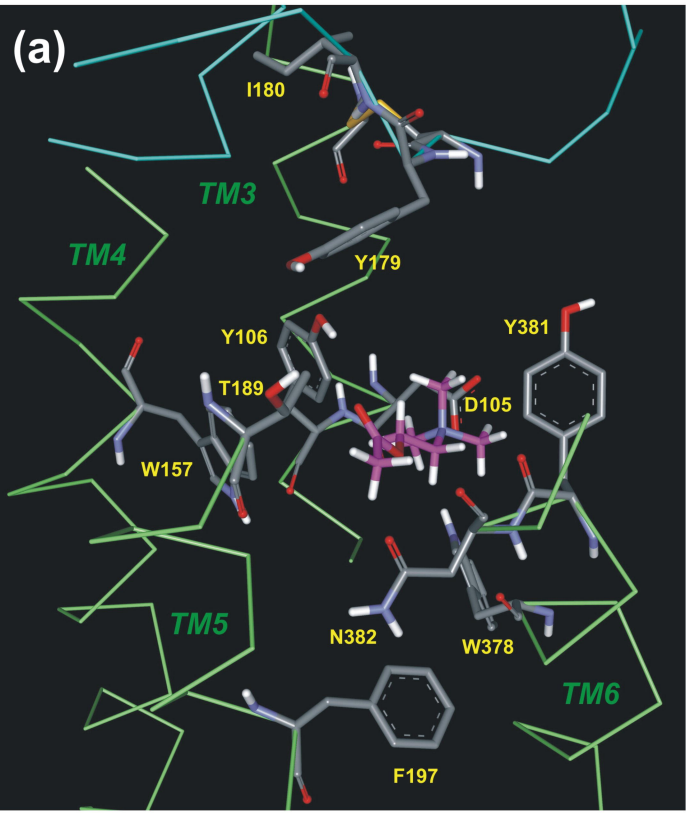

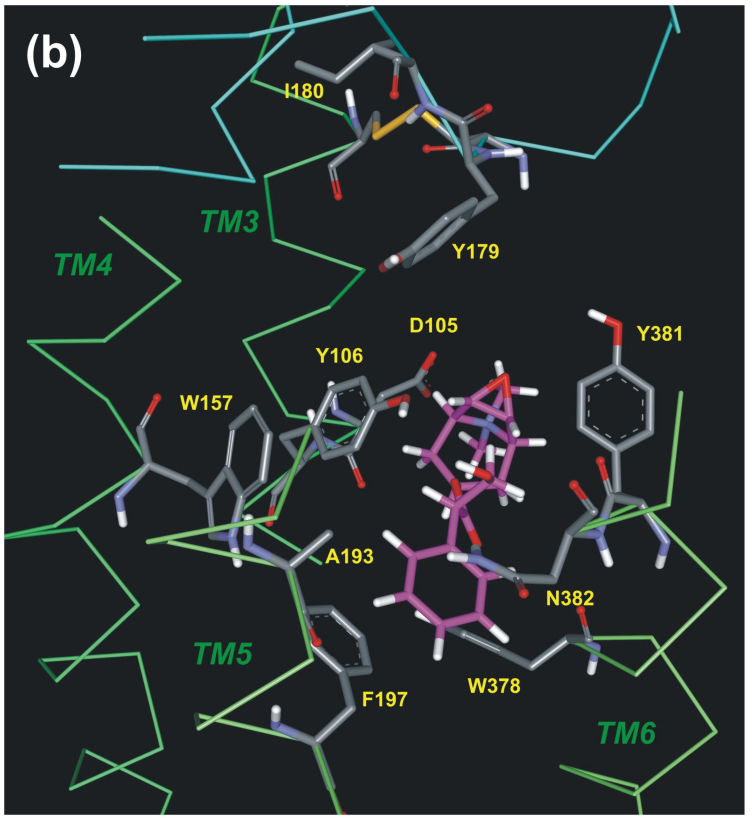

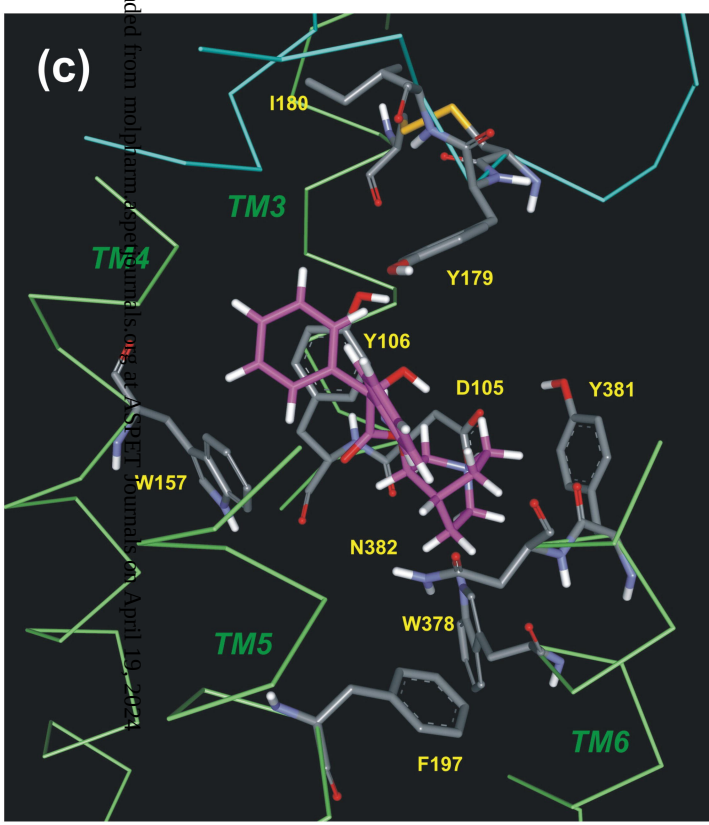

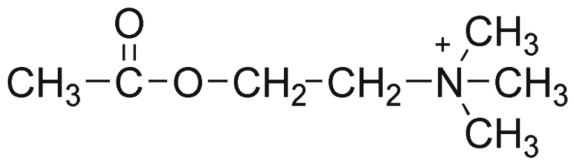

ACh

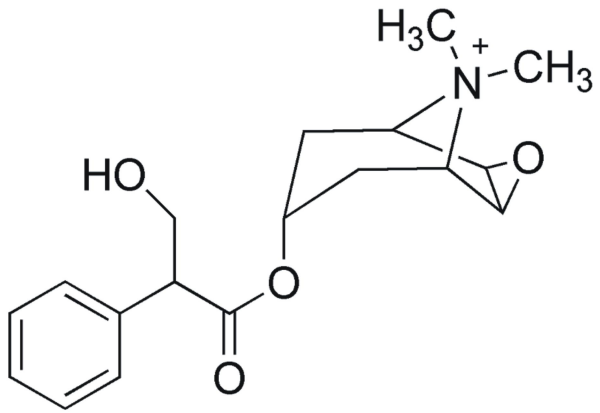

NMS

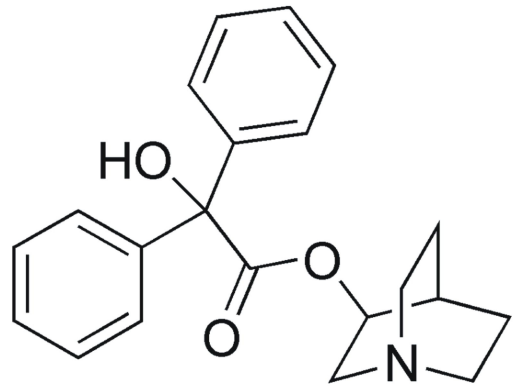

QNB

Molecular Pharmacology Fast Forward. Published on September 11, 2007 as DOI: 10.1124/mol.107.038265
This article has not been copyedited and formatted. The final version may differ from this version.

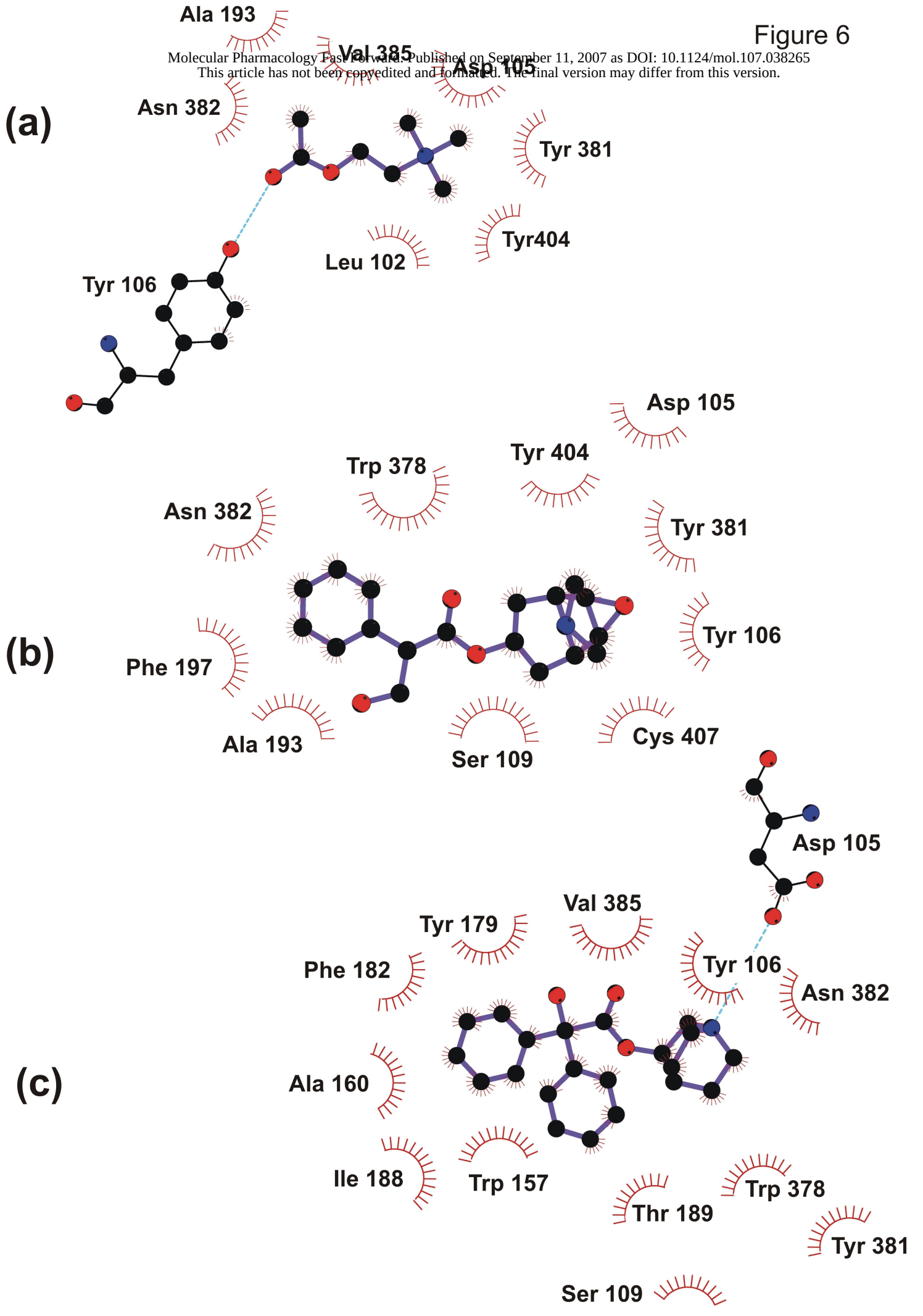

Figure 7

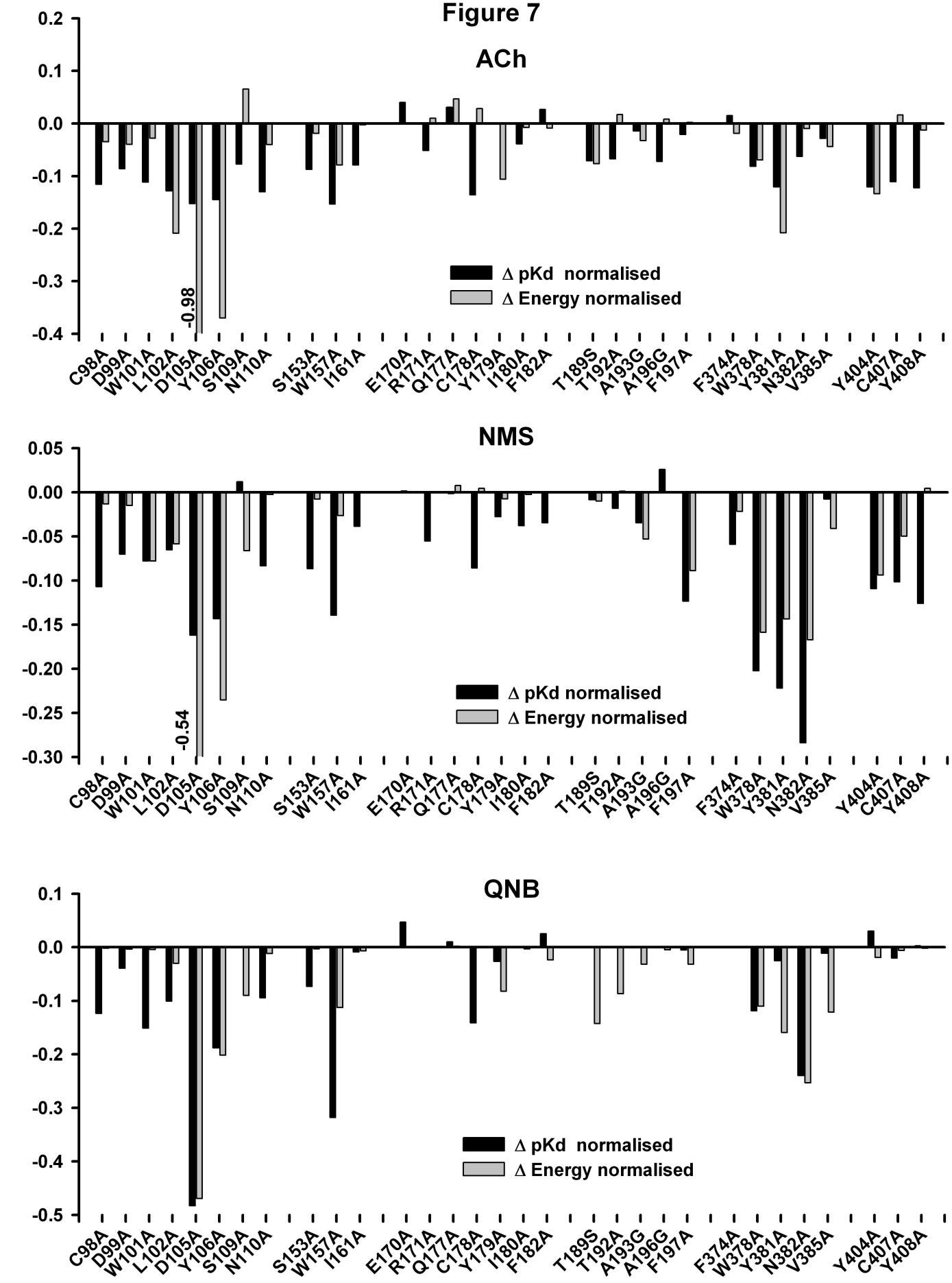
ACh
0.2
0.1
0.0
-0.1
-0.2
-0.3
-0.4
-0.98
Δ pKd normalised
Δ Energy normalised
C98A D99A W101A L102A D105A Y106A S109A N110A S153A W157A I161A E170A R171A Q177A C178A Y179A I180A F182A T189S T192A A193G A196G F197A F374A W378A Y381A N382A V385A Y404A C407A Y408A
NMS
0.05
0.00
-0.05
-0.10
-0.15
-0.20
-0.25
-0.30
-0.54
Δ pKd normalised
Δ Energy normalised
C98A D99A W101A L102A D105A Y106A S109A N110A S153A W157A I161A E170A R171A Q177A C178A Y179A I180A F182A T189S T192A A193G A196G F197A F374A W378A Y381A N382A V385A Y404A C407A Y408A
QNB
0.1
0.0
-0.1
-0.2
-0.3
-0.4
-0.5
Δ pKd normalised
Δ Energy normalised
C98A D99A W101A L102A D105A Y106A S109A N110A S153A W157A I161A E170A R171A Q177A C178A Y179A I180A F182A T189S T192A A193G A196G F197A F374A W378A Y381A N382A V385A Y404A C407A Y408A

Figure 8

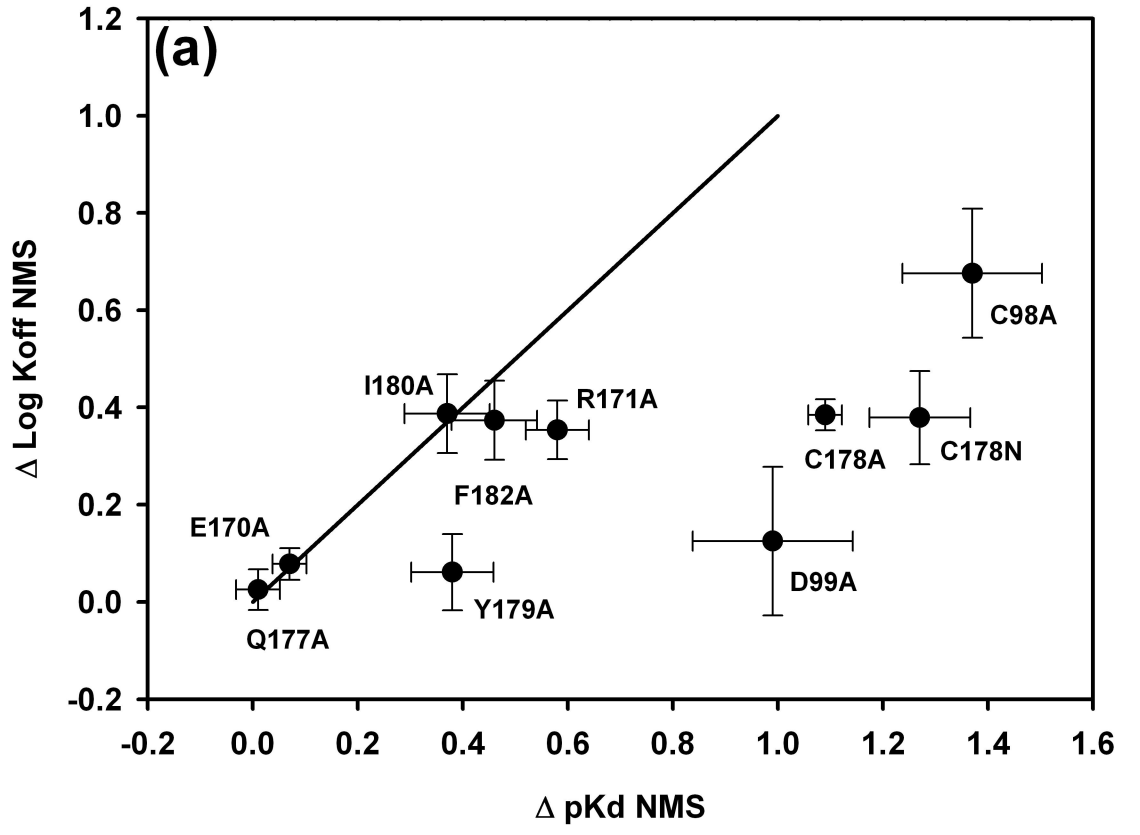
(a)
Δ Log Koff NMS
Δ pKd NMS
1.2
1.0
0.8
0.6
0.4
0.2
0.0
-0.2
-0.2
0.0
0.2
0.4
0.6
0.8
1.0
1.2
1.4
1.6
C98A
I180A
R171A
C178A
C178N
F182A
E170A
D99A
Y179A
Q177A

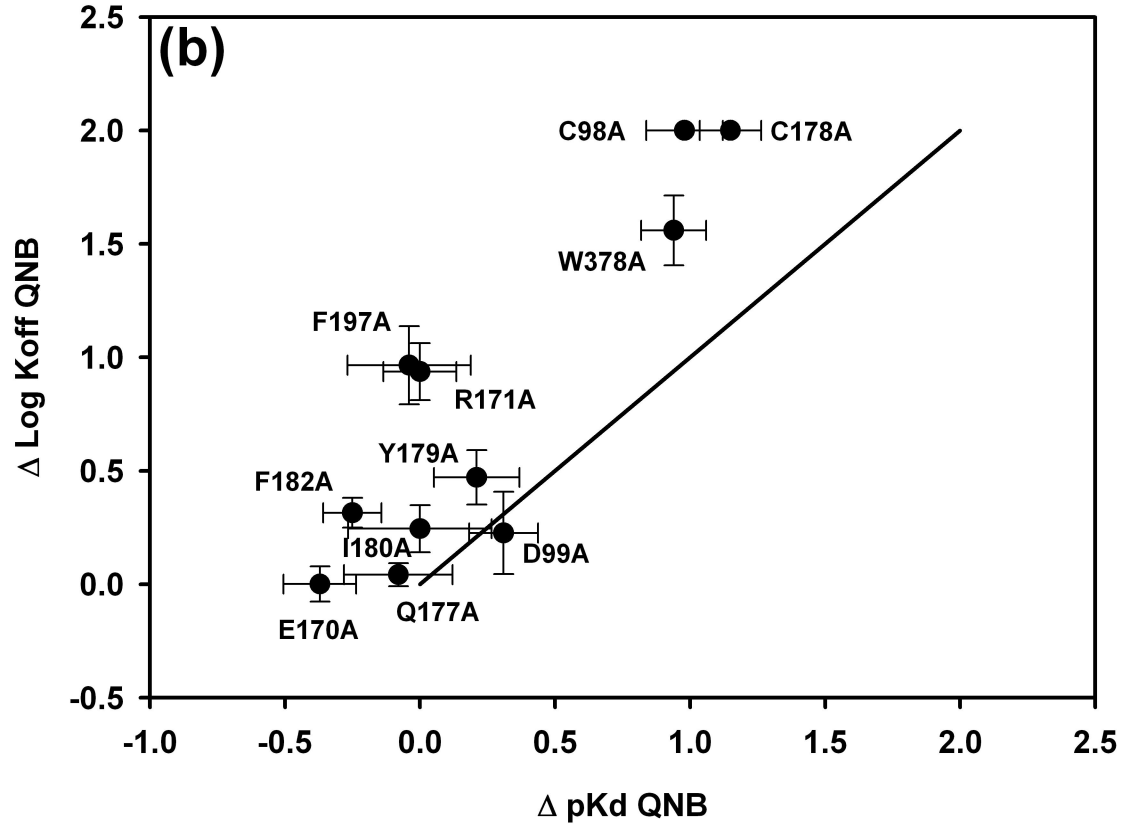
(b)
Δ Log Koff QNB
Δ pKd QNB
2.5
2.0
1.5
1.0
0.5
0.0
-0.5
-1.0
-0.5
0.0
0.5
1.0
1.5
2.0
2.5
C98A
C178A
W378A
F197A
R171A
Y179A
F182A
I180A
D99A
Q177A
E170A